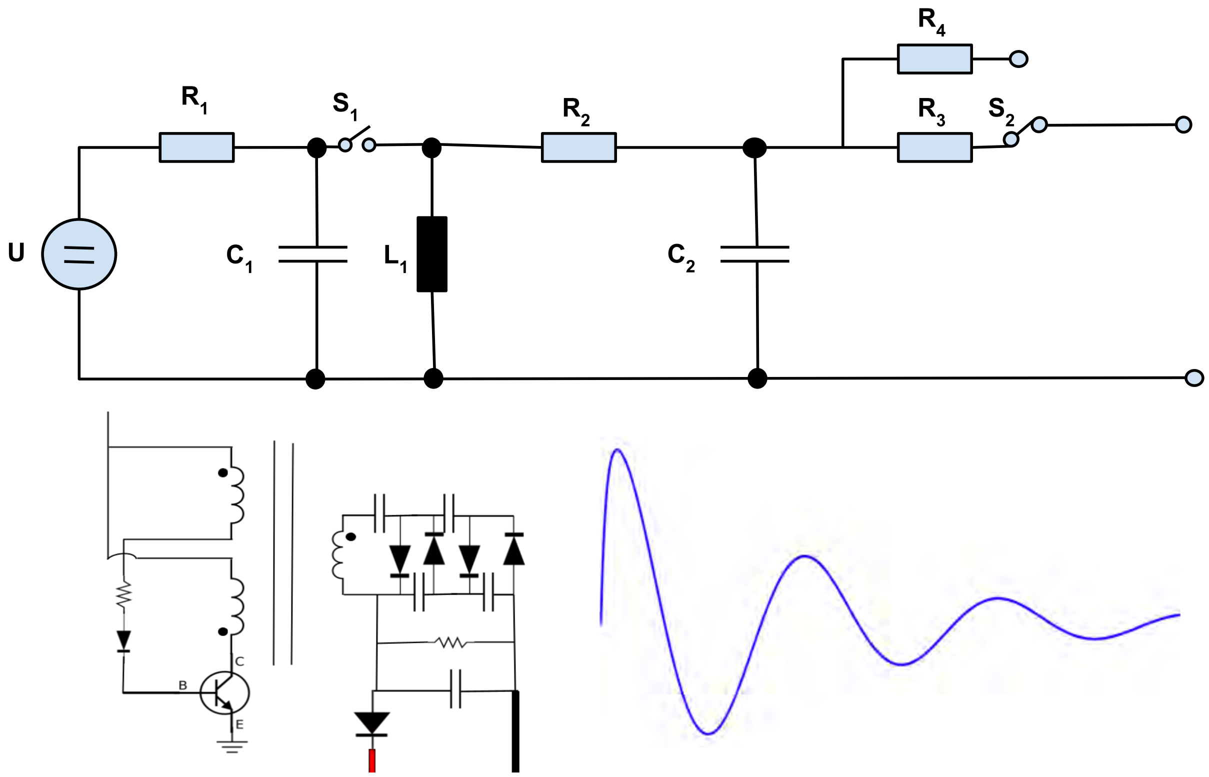

Design and Assembly of a Ring Wave Generator

In accordance with the International Standard IEC 61000-4-12

Master’s thesis in Sustainable Electric Power Engineering and Electromobility

Tobias Ekborg & Albin Björfelt

DEPARTMENT OF ELECTRICAL ENGINEERING
CHALMERS UNIVERSITY OF TECHNOLOGY
Gothenburg, Sweden 2026
www.chalmers.se

Master's thesis 2026

Design and Assembly of a Ring Wave Generator

In accordance with the International Standard IEC 61000-4-12

TOBIAS EKBORG & ALBIN BJÖRFELT

Department of Electrical Engineering
Division of Sustainable Electric Power Engineering and Electromobility
Chalmers University of Technology
Gothenburg, Sweden 2026

Design and Assembly of a Ring Wave Generator
In accordance with the International Standard IEC 61000-4-12
TOBIAS EKBORG & ALBIN BJÖRFELT

Supervisor: Urban Lundgren, Aros Electronics
Supervisor: Dimitrios Meintanis, Aros Electronics
Supervisor: Mangus Wide, Aros Electronics
Examiner: Torbjörn Thiringer, Department of Electrical Engineering

Master's Thesis 2026
Department of Electrical Engineering
Division of Sustainable Electric Power Engineering and Electromobility
Chalmers University of Technology
SE-412 96 Gothenburg
Telephone +46 31 772 1000

Cover: The ring wave circuit, the flyback trigger circuit and a ring wave.

Typeset in LaTeX
Printed by Chalmers Reproservice
Gothenburg, Sweden 2026

Design and Assembly of a Ring Wave Generator
In accordance with the International Standard IEC 61000-4-12
TOBIAS EKBORG & ALBIN BJÖRFELT
Department of Electrical Engineering
Chalmers University of Technology

Abstract

This thesis presents the design and assembly of a ring wave generator developed in accordance with the requirements specified in the international standard IEC 61000-4-12. Component values were determined through analytical calculations and circuit simulations, with all components rated for a 4 kV ring wave output. Procuring a reliable high-voltage switch proved particularly problematic, leading to the implementation of a triggered spark gap utilizing gas discharge tubes. The assembled generator demonstrated low parasitic elements across all components. However, accurately estimating parasitic values in advance proved challenging, resulting in deviations between simulated and measured waveforms. Most notably, and unlike what was observed in simulation, the waveform exhibited minor variations across different voltage levels, particularly in the damping characteristics of the ring wave. Although the measured open-circuit voltage rise time of 720 ns exceeded the standard's limit of 650 ns, all other parameters were successfully met, where frequency was measured between 93.3-96.5 kHz and peak ratios between 0.55-0.8.

Keywords: Ring wave generator, IEC 61000-4-12, electromagnetic compatibility, transient immunity, oscillatory transients, parasitic elements, high voltage, gas discharge tube

Acknowledgements

We would like to express our sincere gratitude to all those who have contributed to and supported us throughout the course of this master's thesis project.

First and foremost, we extend our deepest appreciation to our supervisor, Urban Lundgren, for his invaluable guidance and expertise within the field of electromagnetic compatibility. His constructive feedback, thoughtful design considerations, and assistance in planning and structuring the work have been instrumental in shaping this thesis.

We are also grateful to our examiner, Torbjörn Thiringer, for his dedicated time and effort, and for the constructive feedback provided during our meetings, which greatly contributed to the quality of this work.

Our sincere thanks go to our supervisor, Dimitrios Meintanis, for his hardware expertise and, in particular, for the insightful suggestion to utilize gas discharge tubes in the design of the triggered spark gap. A contribution that proved highly valuable to our project.

A special thanks to our supervisor, Magnus Wide, for providing us the opportunity to carry out this project at Aros. We truly appreciate the trust and the resources provided, which were essential to the success of our study.

Finally, we would like to thank everyone at Aros for their warm welcome and continuous support throughout the project. Their encouragement and assistance made the work both enjoyable and rewarding.

Tobias Ekborg & Albin Björfelt, Gothenburg, May 2026

List of Acronyms

Below is the list of acronyms that have been used throughout this thesis listed in alphabetical order:

AC	Alternating current
CWT	Current waveform transducer
CWTUM	Current waveform transducer ultra mini
DC	Direct current
EMC	Electromagnetic compatibility
ESL	Equivalent series inductance
ESR	Equivalent series resistance
EVM	Evaluation module
GDT	Gas discharge tube
IEC	International Electrotechnical Commission
IEEE	Institute of electrical and electronics engineers
LCD	Liquid crystal display
LED	Light emitting diode
MOSFET	Metal oxide semiconductor field effect transistor
MPL	M-Power-Line
PCB	Printed circuit board
SRF	Self-resonant frequency
UI	User interface

Contents

1
Introduction

1.1 Problem background

Aros Electronics manufactures and designs power electronic solutions to be implemented in various areas, such as vehicles, the power grid and industrial applications. The devices need to comply with electromagnetic compatibility (EMC) regulations according to the IEC 61000 standard series. For devices connected to the power grid, immunity to high-energy transient pulses may be required. One such pulse is the ring wave, characterized by its damped oscillating shape and often produced by nearby lightning strikes, or when large loads or generators are connected/disconnected [1]. Its specific wave shape and compliance tests are specified in IEC 61000-4-12, where a ring wave generator is used to test the effects of such a pulse on grid-connected equipment. However, a ring wave generator is expensive and conducting such tests on-site before doing it at another test site can provide time and financial benefits. Therefore, it can be beneficial for a company engaged with development to build its own generator, in order to test new equipment and make sure it complies with existing standards.

1.2 Previous work

Conference paper [2] explains the design, assembly and testing of a surge- and ring wave generator according to IEC 61000-4-5 [3] and IEC 61000-4-12 [4]. Triggered spark gaps are a good option for high-voltage switches in such generators, research article [5] explains how a triggered spark gap works utilizing gas discharge tubes.

1.3 Purpose

The purpose of this project is to create a ring wave generator that will enable ring wave EMC tests to be conducted on-site at Aros Electronics in Mölndal, potentially providing significant time and financial benefits. The generator should produce a ring wave that meets the requirements defiend by the standard. It should be consistent in different environments and under different loads. It should also be safe, robust and easy for a test engineer to operate.

2
Theory

This chapter introduces concepts and components that have been instrumental in this project, these topics are explained to help facilitate the understanding of the component selection and the results and analysis chapters of this report. Specific measurement instruments and software tools that were used in this project are introduced, and their utilization throughout this project is explained.

2.1 Gas Discharge Tubes

Gas discharge tubes (GDTs) are passive components used to protect circuits and components from overvoltage. GDTs utilize the characteristic of electric gas discharge in gases. When the voltage reaches the threshold voltage of the GDT, a gas discharge or an arc is formed; this rapidly decreases the resistance inside the GDT. Once the overvoltage subsides, the GDT returns to a high-impedance state [6]. A GDT is shown in Figure 2.1. It consists of two metal electrodes separated by a sealed inert gas. The threshold voltage of the GDT can be changed by manufacturers by adjusting the pressure of the gas and distance inside the GDT. GDTs can handle many surges and large currents, and provide a relatively predictable discharge compared to open air discharges [6].

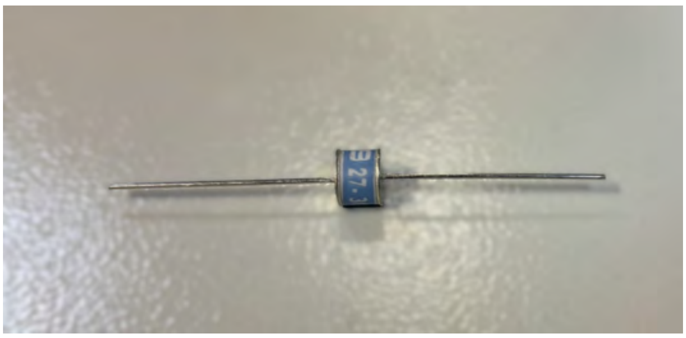

Figure 2.1: A gas discharge tube.

2.2 Triggered spark gap

An ordinary two electrode spark gap can be viewed in Figure 2.2 and it consists of two metal electrodes separated by gas [7]. Under normal conditions, gas is non-conductive; therefore, the electrodes are isolated from each other. This changes if the voltage between the electrodes increases, resulting in an electric field between them, which will accelerate any charges between the electrodes due to the Coulomb force. If the electrons in the gap can gain enough kinetic energy to collide and ionize other molecules in the gap this will lead to a conductive plasma bridging the gap between the electrodes [7]. The triggering of this breakdown is controlled by the voltage between the electrodes and the pressure, according to Paschen's law. By introducing a third electrode the breakdown can be triggered by controlling the voltage on the third electrode. Figure 2.3 shows a three electrode triggered spark gap. The trigger electrode is located in between the two main electrodes and by increasing the voltage on the third electrode until breakdown is reached, the distance will be cut in half between the main electrodes. Which will result in a complete breakdown between the main electrodes [7].

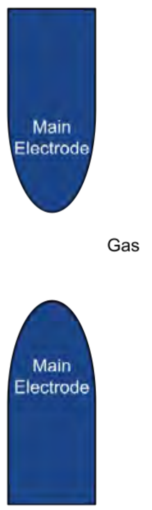

Figure 2.2: Two electrode spark gap.

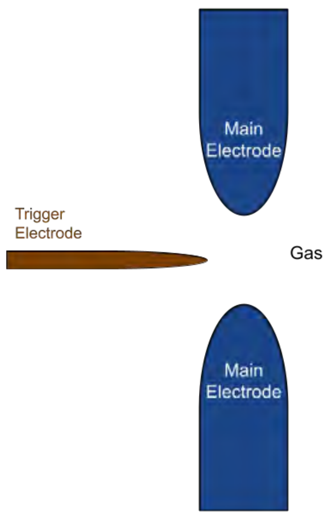

Figure 2.3: Three electrode spark gap.

2.3 Measurement instruments

2.3.1 Capacitor discharge tool

To ensure safe handling of the capacitors a discharge device must be used to manually discharge the capacitors before any work is conducted. A capacitor discharge tool is constructed by connecting a high ohmic resistor of 100 MΩ to high-voltage insulating wires and clamps. A wooden stick is attached to one of the clamps to ensure isolation between the operator and the high-voltage device.

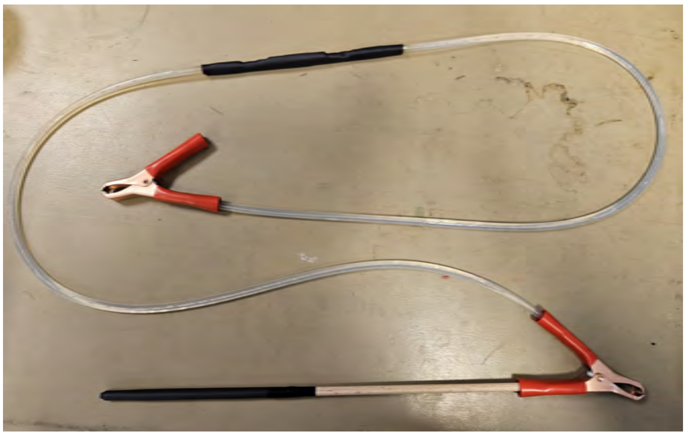

Figure 2.4: The assembled capacitor discharge tool.

2.3.2 Bode 100

A Bode 100, shown in Figure 2.5, was utilized to measure the parameters of the capacitor banks, the inductor and the resistors across different frequencies. This was performed to ensure that the final components had the expected values and get an accurate sense of their parasitics. Furthermore, it improves the simulations by making them more realistic.

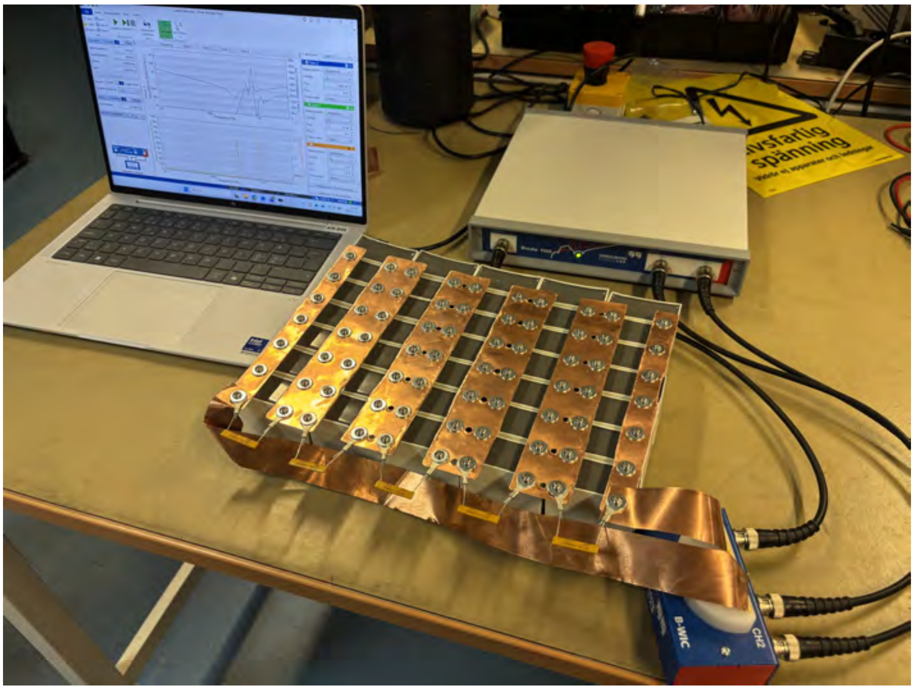

Figure 2.5: Bode 100 setup with the charging capacitor bank.

2.3.3 MPL 1000-10000

In order to produce high-voltage ring waves a high-voltage power source is essential. Different solutions were discussed, but since Aros already obtained a 10 kV source, utilizing it would be the simplest solution. Figure 2.6 shows the MPL 1000-10000 [8], a 1000 W power source. The voltage can be set from 0 to 10 kV and the current can be set from 0 to 100 mA. It can also be controlled through a serial interface, making it suitable for controlling with the microcontroller.

Figure 2.6: 10 kV source used for charging C_1.

2.3.4 CWT Ultra-mini CWTUM/3

The CWT Ultra-mini CWTUM/3 [9] shown in Figure 2.7 was used for current measuring. It can read a 600 A peak current and a current derivative of 40 kA/µs, well above what is required.

Figure 2.7: Rogowski current transducer used for short-circuit current measuring.

2.3.5 Micsig DP20003

The Micsig DP20003 high-voltage differential probe [10] shown in Figure 2.8 was used for open-circuit voltage measurements. It can handle differential voltages up to 5,6 kV and a rise time $\leq$ 3,5 ns.

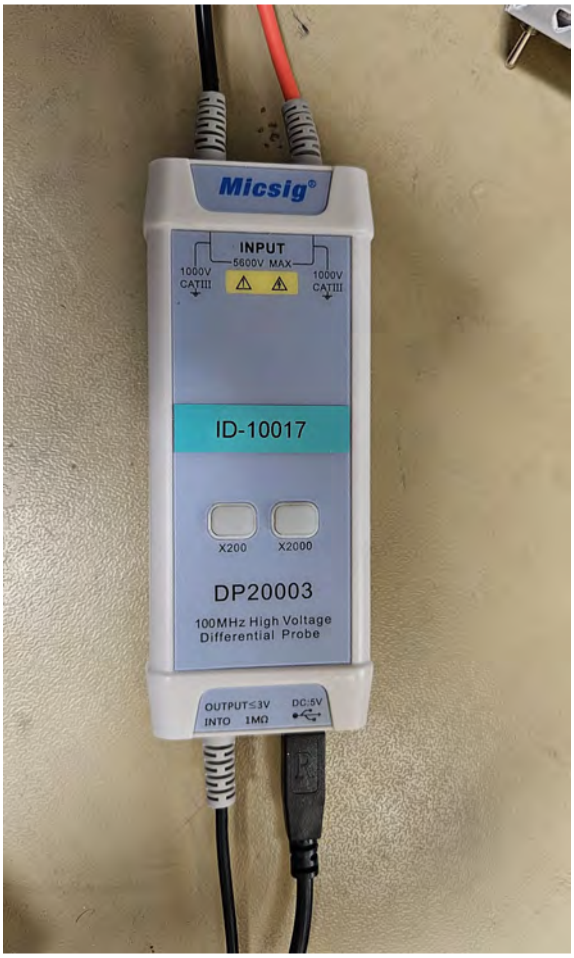

Figure 2.8: The Micsig DP20003 high-voltage differential probe.

2.4 Software tools

The following section presents the software tools used throughout this master's thesis project, outlining the functionality of each tool and their utilization.

2.4.1 LTspice

LTspice is a software tool used for simulation, analysis and verification of analog electronic circuits [11]. It is used in this project to simulate the ring wave circuit and determine component values. The possibility to conduct parameter sweeps has been of particular use in this project.

2.4.2 STM32CubeIDE

STM32CubeIDE is a software tool that allows programming of the microcontrollers from STM32 [12]. The programming language is in C. It is utilized in this project to program the microcontroller.

2.4.3 KiCad

KiCad is a software tool used for electrical schematics and printed circuit board (PCB) design [13]. It is used in this project to create electrical schematics, to improve understanding of the assembled circuits.

2.4.4 MATLAB

MATLAB is a programming and computational program for data analysis, visualization and algorithm development [14]. It has been used in this project to conduct numerical calculations, plot ring waves and simulate design choices.

3

Case setup

To generate a ring wave, a wave-shaping circuit should be used. In IEC 61000-4-12 [4], an example of a ring wave circuit is proposed. The circuit can be viewed in Figure 3.1 and its respective component definitions are given in Table 3.1.

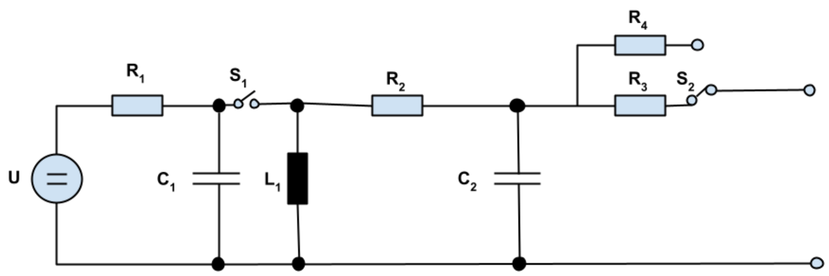

Figure 3.1: Ring wave generator circuit

Table 3.1: Definitions for Figure 3.1

U:	high-voltage source	C_1:	energy storage capacitor
R_1:	charging resistor	C_2:	filter capacitor
R_2:	filter resistor	L_1:	oscillating circuit coil
R_3:	30 Ω resistor	S_1:	high-voltage switch
R_4:	12 Ω resistor	S_2:	output impedance switch

The ring wave circuit consists of components whose values must be determined through calculations and simulations. Once the waveform is satisfactory, components that are well suited for the conditions must be found or constructed. Similarly for the low voltage control circuits. A controller should be used to control the operation of the generator. The performance of the generator needs to be verified through testing.

R_3 and R_4 have been selected to be 12 and 30 Ω according to the standard [4]. The remaining components can be selected freely, provided that the impulse waveform meets the standard requirements. An example of the waveform is shown in Figure 3.2 and the requirements for the final waveform are specified in Table 3.2. The ring wave has a fast rise time, and should oscillate with 100 kHz. The duration of these pulses typically varies between 10 µs and 100 µs.

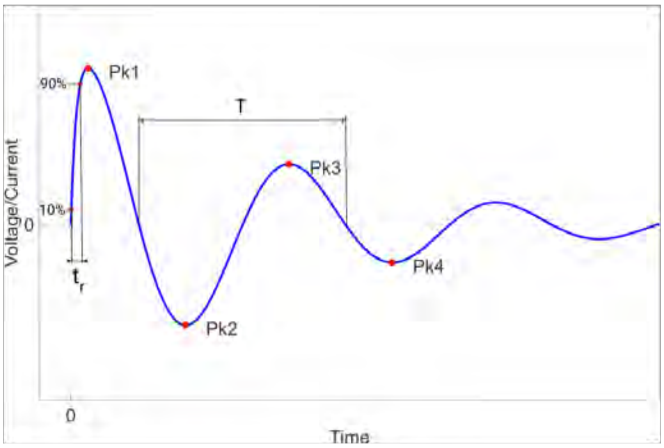

Figure 3.2: Example of the ring wave waveform.

Table 3.2: Table of generator specifications according to standard

Voltage rise time (t_r in Figure 3.2)	0.5 µs ± 30% (Open-circuit condition)
Current rise time (t_r in Figure 3.2)	≤ 1 µs (Short-circuit condition)
Voltage oscillation frequency, Note 1	100 kHz ± 10%
Decaying (Voltage only; see Figure 3.2)	0.4 < Ratio of Pk2 to Pk1 < 1.1 0.4 < Ratio of Pk3 to Pk2 < 0.8 0.4 < Ratio of Pk4 to Pk3 < 0.8 No requirements for other peaks.
Transients' repetition	1 to 60 transients per minute
Output impedance, Note 2	12 Ω and 30 Ω ± 20% (switchable)
Open-circuit voltage (Pk1 value, see Figure 3.2)	250 V to 4 kV (± 10%)
Short-circuit current (Pk1 value, see Figure 3.2)	333 A ± 10% for 12 Ω generator setting 133 A ± 10% for 30 Ω generator setting
Phase relationship with the power frequency	In a range between 0° to 360° relative to the phase angle of the a.c. line voltage to the equipment under test, with a tolerance of ±10%
Polarity of the first half period	Positive and negative

NOTE 1 Oscillation frequency is defined as the reciprocal of the period between the first and third zero crossings after the initial peak, this period is shown as T in Figure 3.2.

NOTE 2 Output impedance is calculated as open-circuit voltage divided by the short-circuit current.

4

Component selection

4.1 Wave-shaping circuit values

The required frequency of the ring wave oscillations is 100 kHz. Thus, the product of L and C can be determined from

$$f_0 = \frac{1}{2\pi\sqrt{LC}} \tag{4.1}$$

where f_0 is the resonance frequency of the system and C is approximately the sum of the capacitance of C_1 and C_2.

The rise time t_r is required to be 0.5 µs ±30% for the voltage during open-circuit condition and ≤ 1 µs for the current during a short-circuit condition. Using $t_\mathrm{r} = 0.5$ µs the product of the RC filter values is determined by,

$$t_\mathrm{r} = 2.2R_2C_2 \tag{4.2}$$

where parameter sweeps were subsequently conducted to achieve the right level of damping of the oscillations. R_2 was therefore chosen to be 1.3 Ω and C_2 was chosen to be 174 nF.

L_1 and C_1 were chosen by parameter sweeps and with (4.1). The final L_1 and C_1 were chosen as $L_1 = 3$ µH and $C_1 = 0.67$ µF. The parameter sweeps were conducted in LTspice and considerations were taken to achieve the standardized waveform.

4.2 Component choices

4.2.1 Capacitor 1

When selecting the physical capacitor for C_1, the objective was to fulfill the requirements and to have a capacitance as close as possible to 670 nF. It must also withstand 6 kV DC voltage, and 3.7 kV peak AC voltage. The oscillating frequency is supposed to be 100 kHz, so the maximum voltage change will be 2.6 kV/µs. The capacitor has to survive 3.6 kA in peak current. Therefore, the final choice became a 470 nF capacitor that is designed for 100 kHz. By placing seven capacitors in parallel and five in series a capacitance of 658 nF is reached. This capacitor bank should according to its datasheet [15] be able to handle 15 kV DC, 5.3 kV AC peak, 6.4 kV/µs and 4.2 kA peak current. Thus, all critical requirements are met as shown in Table 4.1.

Table 4.1: Comparison at 100 kHz

(@100 kHz)	Requirement	YAGEO 0.47 µF
Capacitance	670 nF	658 nF ✓
Vdc	6 kV	15 kV ✓
Vac,pk	3.7 kV	5.3 kV
dV/dt	2.6 kV/µs	6.4 kV/µs ✓
Ipeak	3.6 kA	4.2 kA ✓

4.2.2 Capacitor 2

When choosing a physical capacitor for C_2, the same approach was used. The requirements for this capacitor were that the capacitance should be as close as possible to 174 nF. It should be able to survive 4.4 kV DC and 4.4 kV peak AC. It should also be able to handle 13.1 kV/µs and a peak current of 3.6 kA. The choice is a capacitor from the same series as for C_1 since they are designed for high frequency applications. The capacitance of one capacitor is 330 nF, and by placing four in parallel and seven in series a total capacitance of 188.6 nF is reached. The capacitor bank will be able to handle 21 kV DC, 7.4 kV AC, 14.5 kV/µs, and 4.1 kA peak current according to the datasheet [16]. Therefore, the rating of the capacitor bank exceeds the requirement in all categories, as shown in Table 4.2. The maximum voltage change this capacitor bank should be able to handle is much higher than for C_1 since the voltage rise time t_r should be 0.5 µs for C_2.

Table 4.2: Comparison at 100 kHz

(@100 kHz)	Requirement	YAGEO 0.33 µF
Capacitance	174 nF	188.6 nF ✓
Vdc	4.4 kV	21 kV ✓
Vac,pk	4.4 kV	7.4 kV ✓
dv/dt	13.1 kV/µs	14.5 kV/µs ✓
Ipeak	3.6 kA	4.1 kA ✓

4.2.3 Bleeding and balancing resistors

Bleeding and balancing resistors have also been added to balance the voltage between the capacitors in the banks, and to safely discharge the capacitors over time. The resistor values were chosen according to the discharge time of a capacitor

$$t_{\mathrm{dc}} = -RC \ln\left(\frac{V(t_{\mathrm{dc}})}{V_0}\right) \tag{4.3}$$

where t_{dc} denotes the discharge time, R the resistance, C the capacitance, V_0 the initial capacitor voltage, and $V(t_{\mathrm{dc}})$ the voltage at time t_{dc}. Furthermore, they were chosen so as to not interfere with the pulsed waveform. This was ensured by simulations and parameter sweeps in LTspice. The final value for the balancing and bleeding resistors were chosen to 100 MΩ. The discharge time becomes 28 minutes according to equation 4.3. Although this discharge time is relatively long, the primary purpose is to balance the voltage across the capacitors, and to prevent the capacitor bank from becoming charged while disconnected, for instance through leakage currents or unintended conduction paths such as air ionization. The discharge tool will be used when the banks must be discharged more rapidly.

4.2.4 Resistors 1, 2, 3 and 4

Sourcing resistors that exhibit low resistance, specific values and high voltage ratings is highly challenging. Consequently, the resistors R_2, R_3 and R_4 will be created with resistance wire by using the Ayrton-Perry winding technique to cancel magnetic fields and lower inductance, since these resistors will be part of the high frequency circuit. Resistor R_1 will be created using two 2,5 kΩ resistors in series, each rated for 5 kV. They are placed in series to achieve a high voltage rating and R_1 was chosen to 5 kΩ in order to charge the capacitor bank C_1 in under a second but still isolate the ring wave from the voltage source after the trigger.

4.2.5 Switch 1

The switch S_1 must isolate for voltage levels up to 6 kV, and have a low on-state resistance. Therefore, a triggered spark was selected for switch S_1. The triggered spark gap will use gas discharge tubes (GDTs) instead of open air discharges to improve the predictability, safety and lifetime of the triggered spark gap switch [5]. A proper industrial triggered spark gap is expensive and hard to find, meanwhile GDTs are inexpensive and easy to find at different voltage ratings. However, GDTs have a limited lifetime at certain current levels, specified in their respective datasheets, and can become unreliable after a few discharges [5]. Consequently, they will have to be switched out after some usage. Testing at different voltage levels also require using GDTs with different voltage ratings for it to work. At these moments they will also have to be switched out. Figure 4.1 shows a schematic of a triggered spark gap.

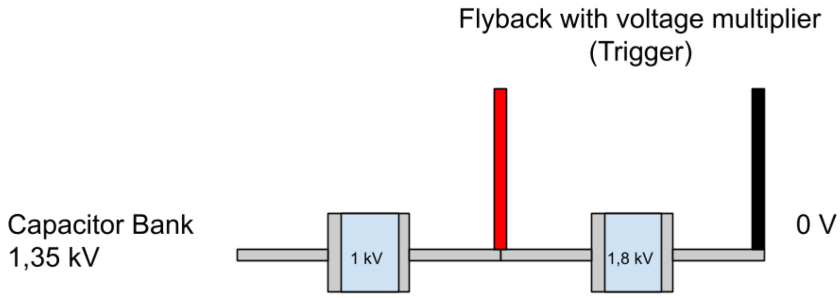

Figure 4.1: Schematic of a triggered spark gap consisting of two GDTs and flyback trigger connections.

As shown in Figure 4.1 one GDT should have a breakdown voltage below the charged capacitor bank, and the other GDT should be above to ensure that only the trigger electrode can create a complete breakdown. Therefore, a triggered spark gap requires a high-voltage source that can trigger a discharge.

4.2.5.1 Flyback trigger

The high-voltage source used in this project is a flyback converter with a very high winding ratio, the schematic of the entire flyback setup is shown in Figure 4.2.

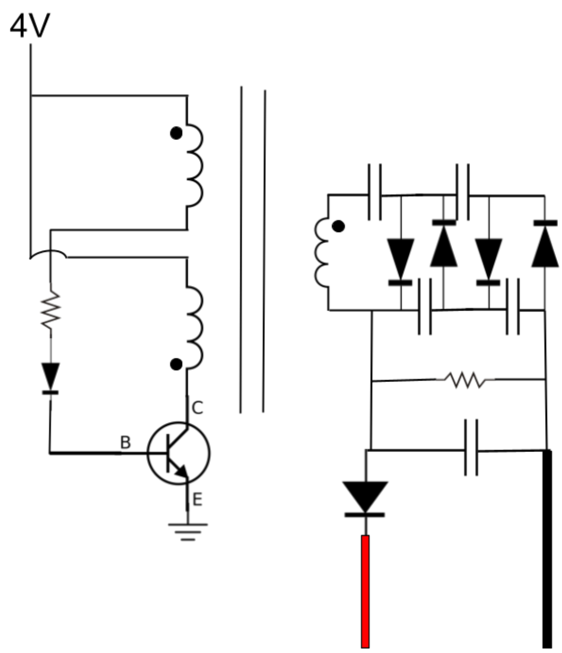

Figure 4.2: Schematic of the flyback converter with a voltage quadrupler and output capacitor.

As shown in Figure 4.2 the flyback converter is connected to a voltage multiplier to turn the voltage from AC to DC and to increase the voltage further. The voltage multiplier consists of four multiplier stages, which results in a voltage quadrupler. The voltage quadrupler has a 2.5 nF output capacitor that will be discharged over the GDT to trigger the spark gap. Since the output capacitance is small, the capacitor gets charged quickly and can therefore be controlled precisely by initiating a short pulse.

4.2.6 GDT combinations

In order to produce ring waves at varying voltage levels, different GDT combinations must be utilized. Table 4.3 shows the GDT combinations used in this project.

Table 4.3: GDT combinations for different voltage levels

Capacitor bank voltage	GDT 1	GDT 2	Ring wave level
320 V	250 V	420 V	**250 V**
630 V	500 V	800 V	**500 V**
1.35 kV	1 kV	1.8 kV	**1 kV**
2.63 kV	2 kV	3.5 kV	**2 kV**
5.5 kV	4.5 kV	7.2 kV	**4 kV**

Due to damping in the ring wave circuit the capacitor bank voltage always has to be higher than the ring wave level. The GDT combinations were chosen so that the capacitor bank voltage can break down GDT 1, but not GDT 2. This ensures that only the flyback can trigger the spark gap. The GDTs tolerances were also taken into account, since manufacturers often specifies a 15-20% tolerance for GDTs.

4.2.7 Switch 2

Switch S_2 should have the ability to select between the two output resistors. Therefore, two reed relays were chosen as switch. Reed relays are activated by sending a current through its internal coil, which creates a magnetic field to close the switch. Thus, the turn-on signal is galvanically isolated from the switch. These particular relay coils are powered at 5 V and have a coil-to-contact isolation of 17 kV according to the datasheet [17], making them excellent for high-voltage switching with a controller.

4.2.8 Inductor

The inductor should be made to achieve an inductance of 3 μH. It must handle high voltage and high current pulses. The large voltage across it could lead to breakdown, thus proper insulation needs to be applied. The large current leads to two problems, saturation of the core and large magnetic forces. It should also be made to minimize the influence of the skin effect.

To completely remove the risk of saturation an air core is used. For air core inductors the inductance of a single layer coil can be calculated using Wheeler's formula

$$L = \frac{N^2 r^2}{8r + 11l} \tag{4.4}$$

where N is the number of wire turns, r is the mean coil radius in inches and l is the length of the coil in inches [18].

To keep the resistance of the inductor low the skin effect needs to be mitigated. The skin depth is approximated as

$$\delta = \sqrt{\frac{\rho}{\pi f \mu_r \mu_0}} \tag{4.5}$$

where ρ is the resistivity of the conductor material, f is the frequency, μ_r is the relative permeability of the conductor material and μ_0 is the permeability of vacuum. The skin depth in copper at 100 kHz is approximately 0.2 mm. Thus, using litz wire with 120 strands of 0.1 mm in diameter should remove the skin effect. The wire is coated in polyurethane which should have sufficient turn-to-turn dielectric strength if the coil has more than 12 turns.

4.2.8.1 Inductor forces

The main forces acting on the coil are the axial pressure and the radial expansion, as seen in Figure 4.3.

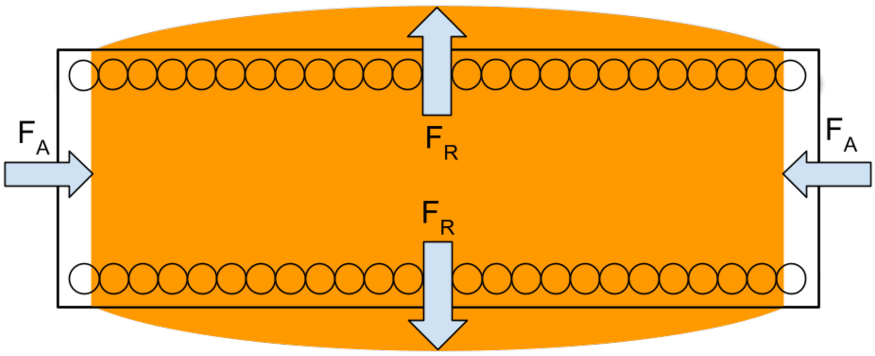

Figure 4.3: Cross section view of the original (white rectangle) and deformed inductor geometry (orange) due to magnetic forces.

The large current produces a strong magnetic field in the inductor, leading to an internal radial force F_R that expands the windings outward and an outer axial force F_A compressing the coil windings. The radial expansion will also lead to circumferential hoop stress that wants to rip the coil apart [18]. The axial and radial forces can be approximated as

$$F = \frac{1}{2}\frac{\mathrm{d}L}{\mathrm{d}x}\hat{I}^2 \tag{4.6}$$

where $\frac{\mathrm{d}L}{\mathrm{d}x}$ is the change of inductance due to a small coil size variation in a certain direction and $\hat{I}$ is the peak current [18]. To minimize the winding movement due to the forces, the wire is tightly wound around a fiberglass bobbin and reinforced with fiberglass filament tape wound around the coil circumference. To further improve the mechanical stability of the coil, it can be vacuum-potted in epoxy resin [18].

The hoop stress in the tape can be approximated as

$$F_\mathrm{hoop} = \frac{F_\mathrm{R}}{2\pi} \tag{4.7}$$

[18]. Furthermore, the radial expansion of a cylinder due to a uniform radial pressure can be approximated as

$$\Delta r = \frac{qr^2}{Et} \tag{4.8}$$

$$q = \frac{F_\mathrm{R}}{A} \tag{4.9}$$

where q is the force per unit area, E is the modulus of elasticity for the cylinder material, t is the cylinder wall thickness and A is the area of the cylinder circumference [19].

Using a 1% change of coil radius and a simulated current of 2.2 kA, the radial force F_R was calculated to be 530 N. The axial force was calculated to be 266 N. This will result in a hoop stress of approximately 0.84 N/cm.

4.2.8.2 Inductor parasitic capacitance

The inductor produces some interturn parasitic capacitance. The total parasitic capacitance can be calculated as

$$C_\mathrm{s} = \frac{2\epsilon_0\pi^2 r}{(N-1)\ln[\frac{p_\mathrm{t}}{d} + \sqrt{\frac{p_\mathrm{t}}{d}^2 - 1}]} \tag{4.10}$$

where p_t is the turn-to-turn distance and d is the wire diameter [20]. Using 4.10 results in approximately 263 pF of total parasitic capacitance in the inductor.

4.3 Generator assembly considerations

4.3.1 Wiring

The high-voltage components will be bolted and connected through thin copper buses or litz wire. The copper buses will be 0.5 mm thick, but a few centimeters wide. This will ensure low resistance and good utilization of the conduction material, considering the skin effect at 100 kHz.

4.3.2 Ground and earthing connections

To ensure low impedance ground and earth connections copper grounding braids are used. Protective earth is connected to the chassis of the generator.

4.3.3 Isolation distances

Since the generator chassis is grounded all components in the ring wave circuit has to be sufficiently isolated from the ground plane to avoid undesired discharges. If C_1 is charged to 6 kV a discharge can occur over an approximate 2 mm distance. A minimum distance of 1 cm should be sufficient, but preferably even more. Measures are taken to reduce too tight spaces. Components connected with cable lugs to standoff legs will use either plastic standoff legs or plastic screws in the bottom, in order to remove the risk of discharge to the ground plate.

5

Results and Analysis

5.1 Capacitor 1

The assembled charging capacitor bank C_1 is shown in Figure 5.1.

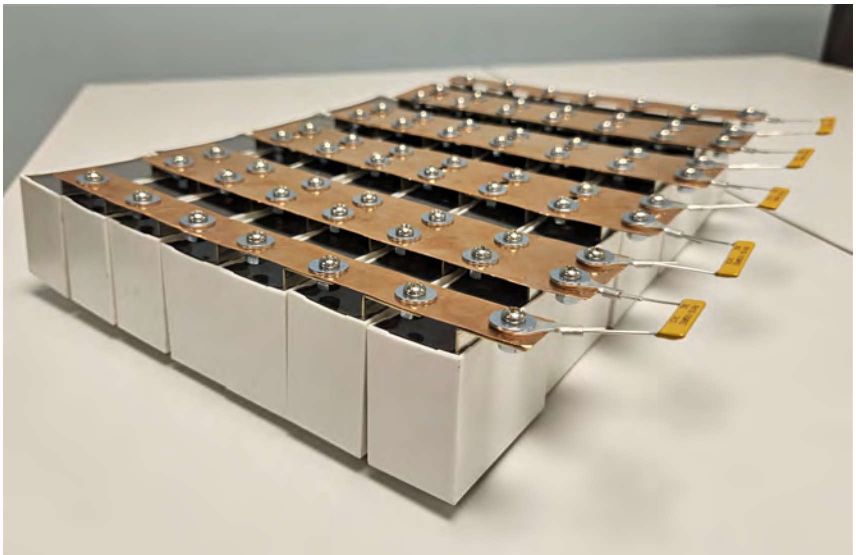

Figure 5.1: High-voltage capacitors bolted to copper buses with bleeding resistors to make up the 666 nF charging capacitor bank C_1, designed for 15 kV DC.

As described in 4.2.1, seven capacitors are placed in parallel and five in series to surpass the requirements. They are bolted with screws to copper busbars and bleeding resistors are attached to keep them discharged when not in use.

Capacitance and series resistance measurements were conducted on the bank with a Bode 100 to ensure correct values. The results are shown in Figure 5.2 and Figure 5.3.

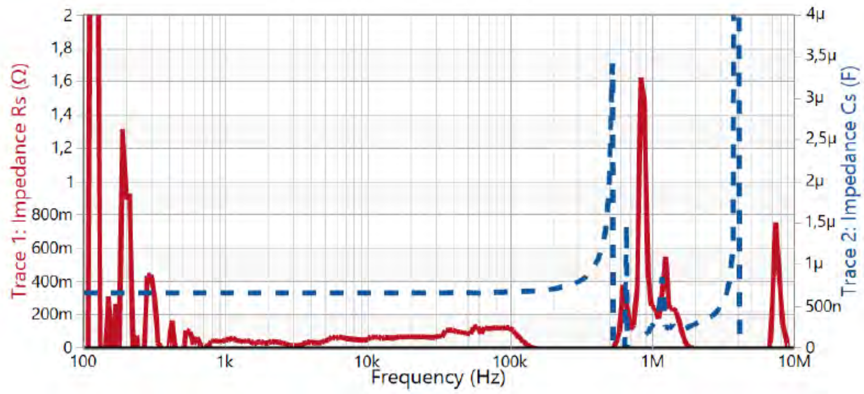

Figure 5.2: Charging capacitor bank Bode measurement of capacitance and series resistance.

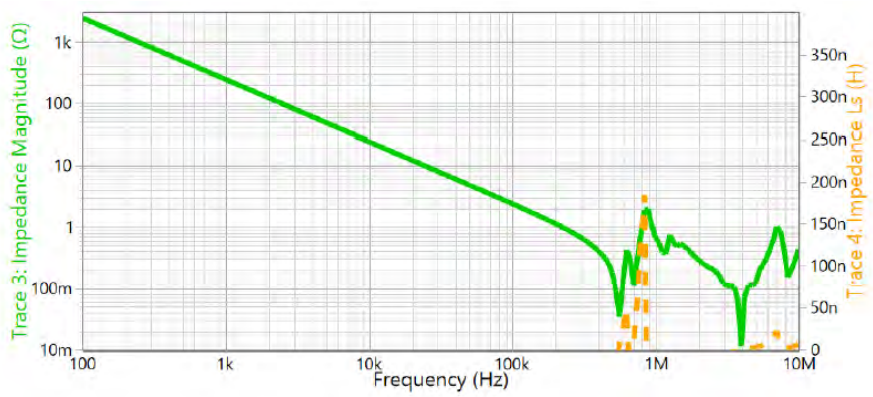

Figure 5.3: Charging capacitor bank Bode measurements of impedance and inductance.

At the ring wave oscillating frequency of 100 kHz, the capacitance was measured to 666.4 nF and the series resistance was measured to approximately 117.6 mΩ. However, the equivalent series resistance (ESR) is found at the self-resonant frequency (SRF) of the impedance, since this is the point where the inductive and capacitive reactances cancel each other. Self-resonance occurs at approximately 560 kHz and the ESR is around 25.2 mΩ. The equivalent series inductance (ESL) of the bank is calculated using (4.1) and the SRF to be around 121 nH.

5.2 Capacitor 2

The assembled filter capacitor bank C_2 is shown in Figure 5.4.

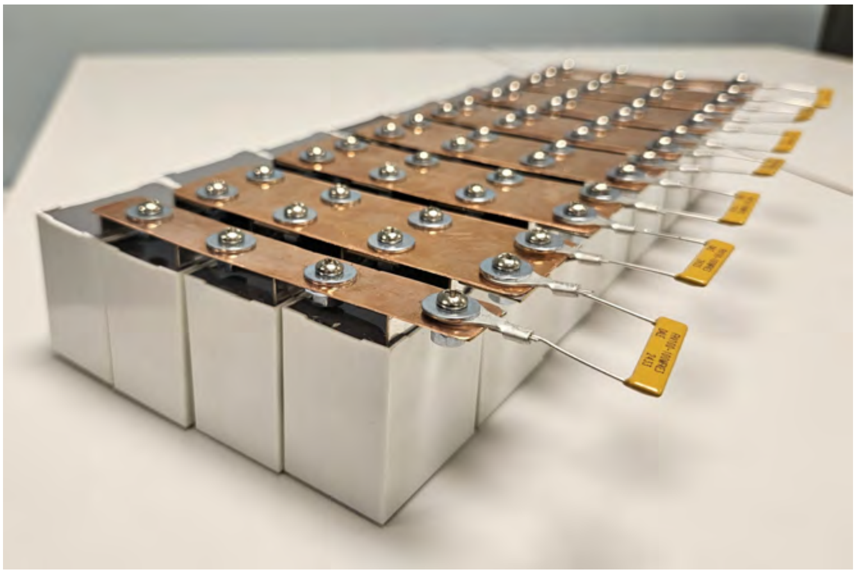

Figure 5.4: High-voltage capacitors bolted to copper buses with bleeding resistors to make up the 188 nF filter capacitor bank C_2, designed for 21 kV DC.

Just like the charging bank, the filter bank is bolted to copper busbars and bleeder resistors are attached. This bank uses four capacitors in parallel and seven in series. The measurements on this bank are shown in Figure 5.5 and Figure 5.6.

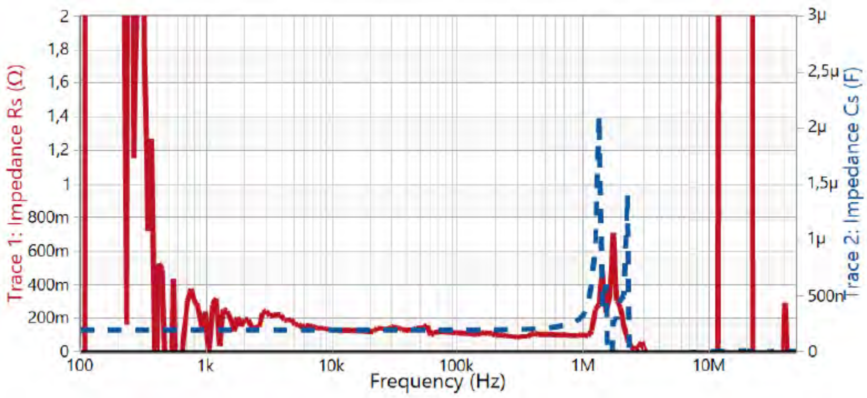

Figure 5.5: Filter capacitor bank Bode measurements of capacitance and series resistance.

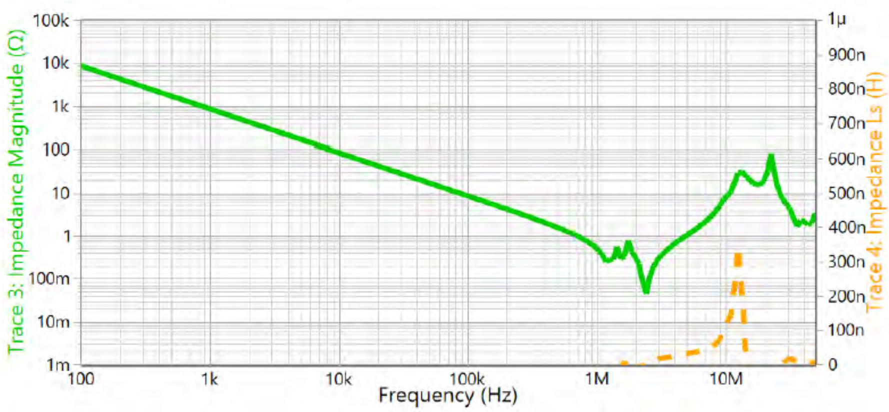

Figure 5.6: Filter capacitor bank Bode measurements of impedance and inductance.

The capacitance of the filter capacitor bank was measured to be 188.3 nF at 100 kHz. The SRF of the filter bank happens approximately 1.5 MHz and using (4.1) the ESL was found to be around 64.4 nH. The ESR is difficult to tell from the measurements, but it is approximately 50 mΩ.

Further improvements could be made to both capacitor banks for better overall generator performance. Both capacitor banks have long distances between their respective positive and negative nodes, making wired connections quite long. If the banks could be made with shorter connection distances between the nodes, resistance and parasitic inductance would be lowered.

5.3 Resistor 1

The assembled and connected charging resistors are shown in Figure 5.7.

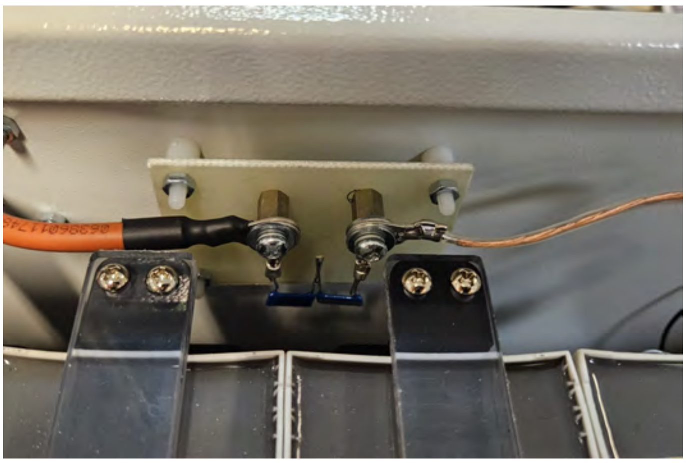

Figure 5.7: Two 2,5 kΩ charging resistors, rated 5 kV each, attached to the generator chassis wall and connected to the charging capacitor bank and the input high-voltage source.

The two resistors are soldered together and connected with cable lugs to standoff legs. Here the high-voltage source and charging capacitor bank are also connected. The standoff legs are attached to the platform with plastic screws on the bottom. The platform is attached to the chassis wall using plastic standoff legs and screws. Sufficient distance from ground is very important here, since the charge voltage is supplied at this stage.

5.4 Switch 1

Figure 5.8 and 5.9 show how the GDTs are placed and connected.

Figure 5.8: View of GDT connections on platform and labels for easier understanding of connections.

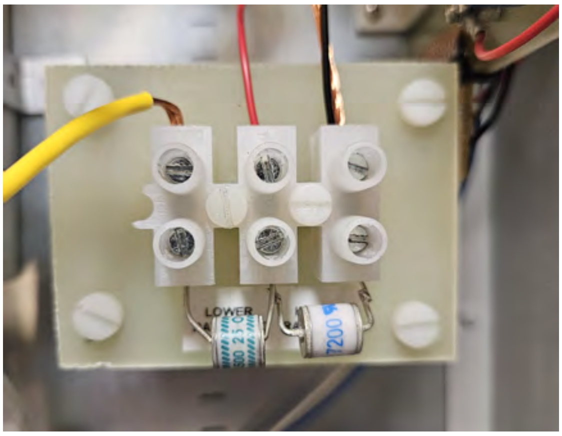

Figure 5.9: Top view of GDTs connected to the charging capacitor bank (Yellow wire), the inductor and filter resistor (Copper wire), and the flyback trigger (Red and Black wires).

The GDTs are fixed inside screw terminals on top of a platform, made from PCB material, with tall standoff legs for easy access when changing the GDTs and to reduce the risk of touching any potentially powered conductor. The other connecting wires are fixed on the opposite side of the screw connectors to prevent accidental disconnection when changing GDTs. The platform is labeled in order to make the connections easier to understand and lower the risk of accidental misplacement.

5.4.1 Flyback trigger

To trigger switch S_1 a high-voltage source is needed. In this case, a flyback converter with a voltage quadrupler is used, as shown in Figure 5.10. The flyback converter can be viewed in the solid rectangle. The voltage multiplier in the dashed rectangle and the output capacitors, resistors and diode are shown inside the dotted rectangle. Figure 5.11 shows the corresponding schematic, where the solid rectangle surrounds the flyback converter, the dashed line shows the voltage multiplier and the dotted line shows the output capacitor, resistor and diode.

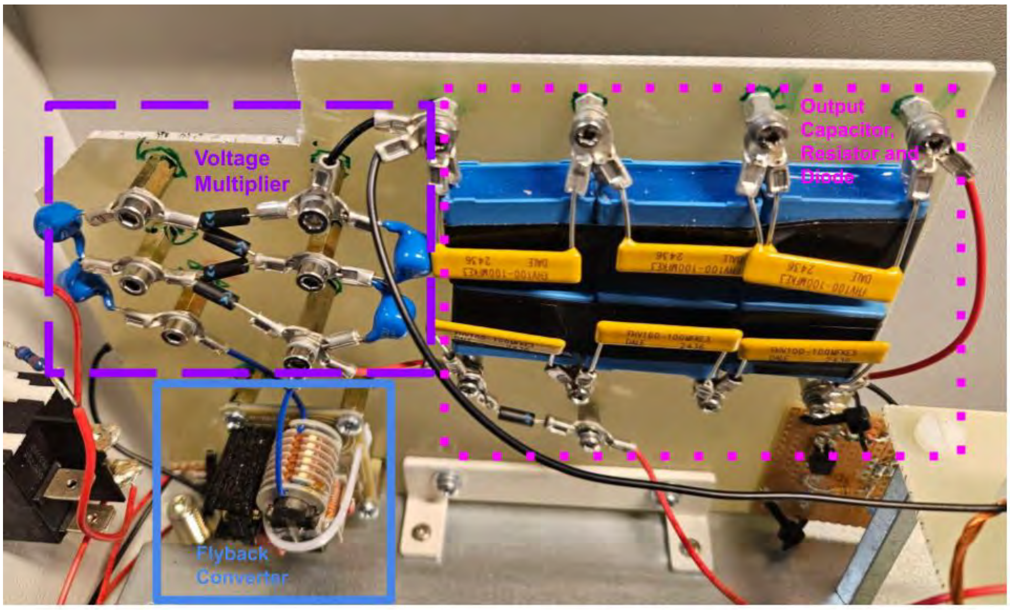

Figure 5.10: Flyback converter with voltage quadrupler and output capacitors.

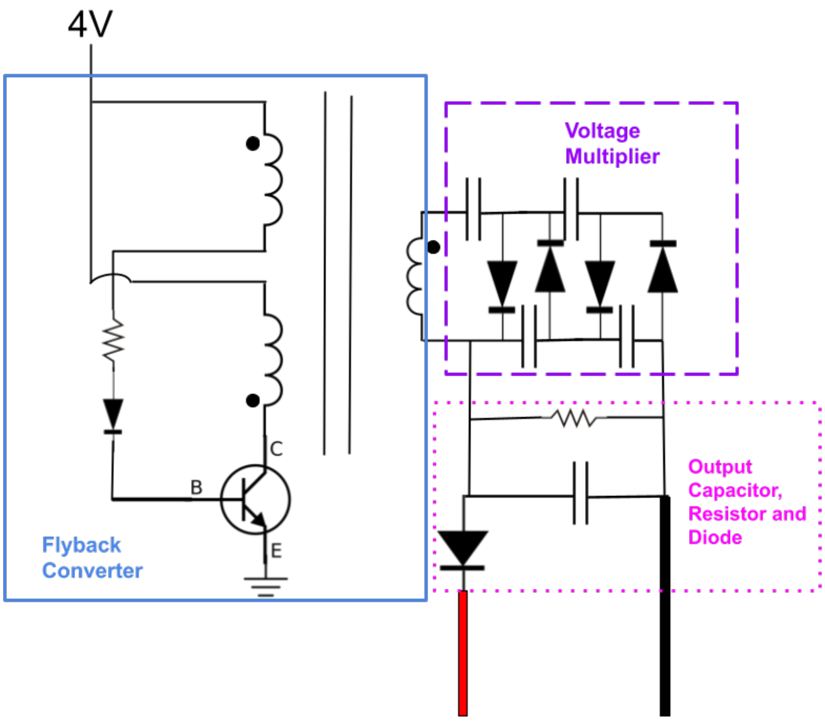

Figure 5.11: Schematic of the flyback converter with voltage multiplier and output capacitors.

5.5 Resistor 2

The constructed filter resistor can be viewed in Figure 5.12.

Figure 5.12: The 1.3 Ω filter resistor, made from nichrome wire wound around a fiberglass tube using the Ayrton-Perry winding method, and is designed for 10 kV.

It consists of a fiberglass tube with an air core. Nichrome wire is then wound around the fiberglass tube. The nichrome wire is wound around the core like two inductors, but wound in opposite directions so that the magnetic fields will cancel each other. This results in a very low inductance for the resistor. The two windings start and end at the same place and are connected at these points by the cable lugs. This means that the potential between the windings will be approximately the same along the entire windings and therefore, parasitic capacitance should be minimized by this winding technique. From the SRF the parallel capacitance is calculated to be 730 pF. This is called the Ayrton-Perry winding technique and it is particularly good for high frequency applications [22]. As can be seen in Figure 5.13 the impedance of the filter resistor is approximately 1.3 Ω for all frequencies except above 1 MHz. This occurs because the Bode 100 measures the inductance to be only 80 nH.

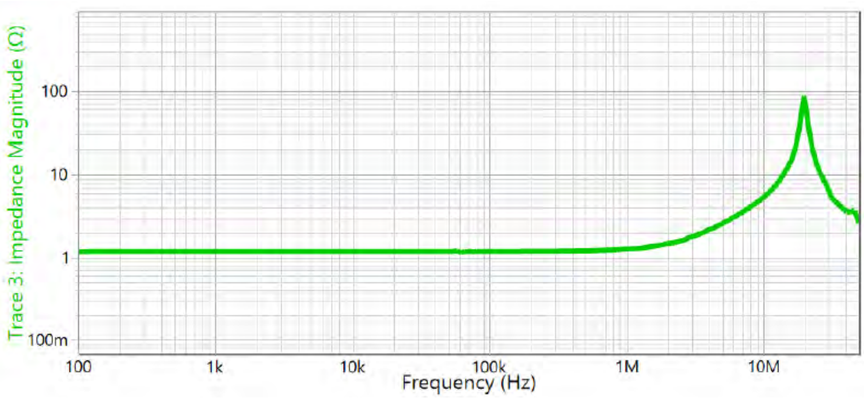

Figure 5.13: Filter resistor impedance for frequencies from 100 Hz to 50 MHz.

5.6 Inductor

The final assembled inductor is shown in Figure 5.14.

Figure 5.14: Litz wire wound around a fiberglass tube and wrapped with fiberglass tape to make up the 2.7 µH air core inductor, designed for 5 kA.

Litz wire is wound tightly around a hollow, air-core fiberglass tube. Zip ties are placed on each end to keep the turns packed close together and glass fiber filament tape is wrapped over the windings to lock them in place and increase the mechanical stability. The tensile strength of the tape is 280 N/cm, far more than the calculated force of 0.84 N/cm that the inductor will be exposed to. Each end of the wire is stripped from its coating and tinned for good electrical connection. The Bode 100 measurements on the inductor are shown in Figure 5.15.

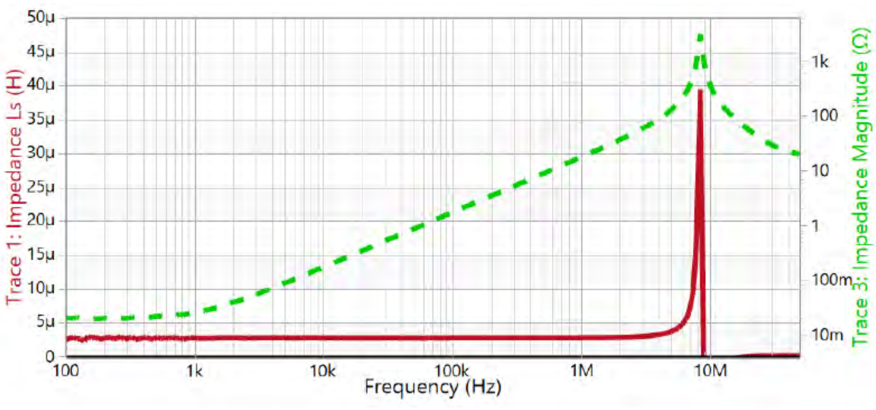

Figure 5.15: Inductor Bode measurements of impedance and inductance across the frequency spectrum, with an SRF of 8.5 MHz.

At 100 kHz the inductor measures 2.7 µH in inductance. The SRF happens around 8.5 MHz. The series resistance is calculated to be around 24 mΩ. Using (4.1) and the SRF of the inductor, the parasitic capacitance can be calculated. The parasitic capacitance is approximately 130 pF, which is half of the calculated in 4.2.8.2.

5.7 Resistor 3 and 4

Figure 5.16 and Figure 5.17 show the final output resistors, while Figure 5.18 illustrates how the resistors were wound.

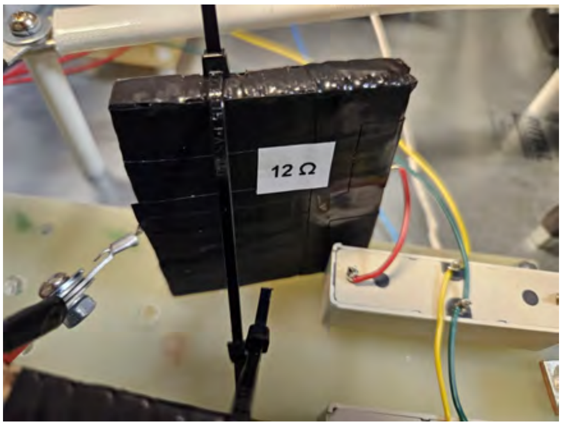

Figure 5.16: The wire wound 12 Ω resistor, designed for 20 kV. Connected to a reed relay and the positive output.

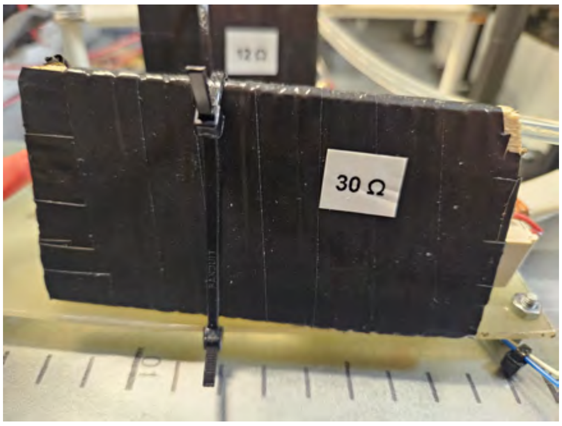

Figure 5.17: The wire wound 30 Ω resistor, designed for 20 kV. Connected to a reed relay and the positive output.

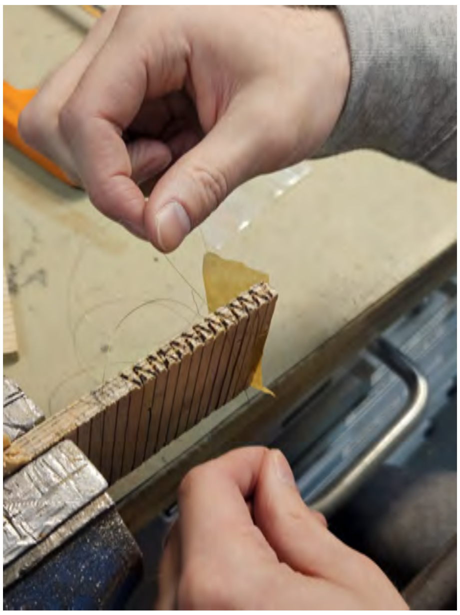

Figure 5.18: Ayrton-Perry winding procedure of the 12 Ω resistor.

Both of the 12 Ω and the 30 Ω resistors were wound with the Ayrton-Perry winding method using 28 Ω/m resistance wire. The wire was wound around a non-metallic square body and taped for stability. A Bode 100 measurement of the 12 Ω resistor is shown in Figure 5.19.

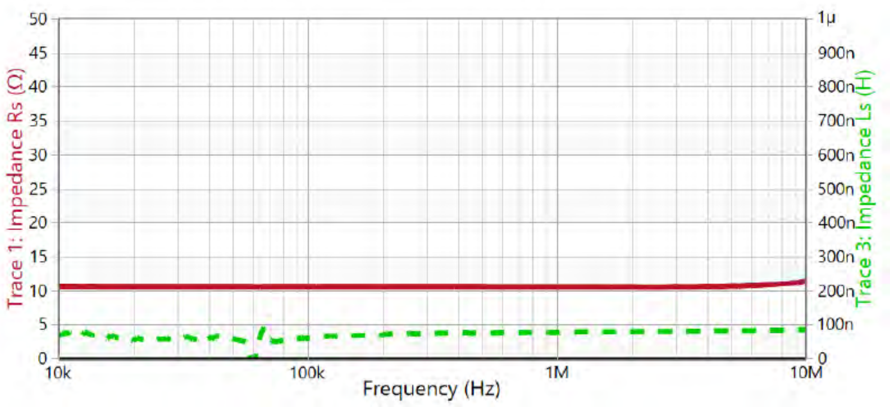

Figure 5.19: Bode measurements of the 12 Ω resistor.

The measurements show a resistance value of 10.5 Ω and 59.3 nH at 100 kHz. Measuring the resistance with a multimeter shows a resistance of exactly 12 Ω. The 30 Ω resistor was measured to 29.8 Ω with a multimeter.
All self-made resistors could be improved in the future. The 12 and 30 Ω resistors use very thin resistance wire, making their connection points fragile. These resistors, along with the filter resistor, are also large and bulky. Thus, reducing their size and employing thicker wire would be a significant improvement.

5.8 Switch 2

The reed relays are shown in Figure 5.20.

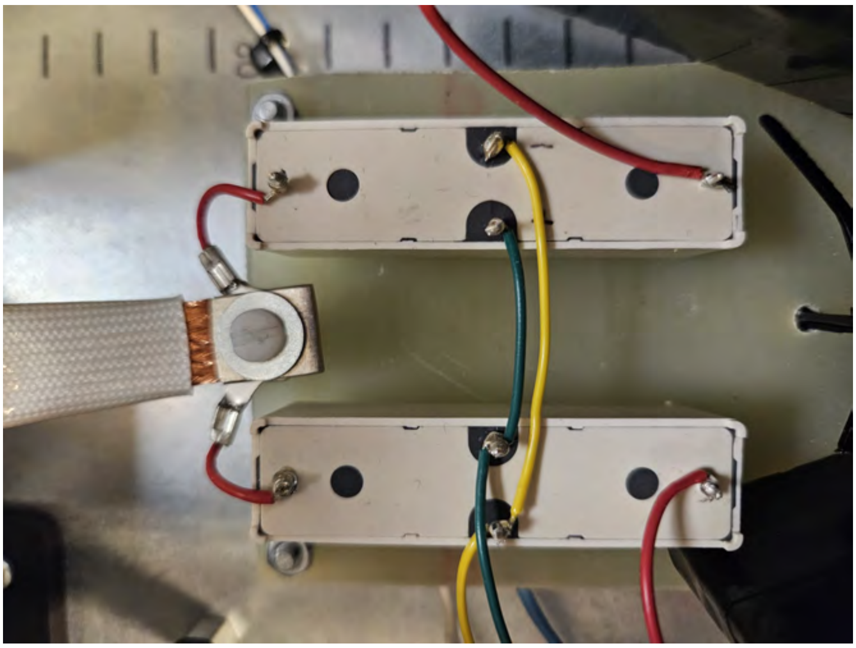

Figure 5.20: Reed relays connected to the ring wave circuit (red wires) and the control circuit (green and yellow wires).

The relays are connected to the ring wave circuit through the red wires. One side of the relays is connected to each respective output resistor, while the other side of both relays is connected to the filter capacitor bank. The green wire is connected to the positive side of a 5 V drive circuit, and the yellow wire is connected to the negative side of the same circuit. The connections are shown in Figure 5.21 and its schematic is shown in Figure 5.22.

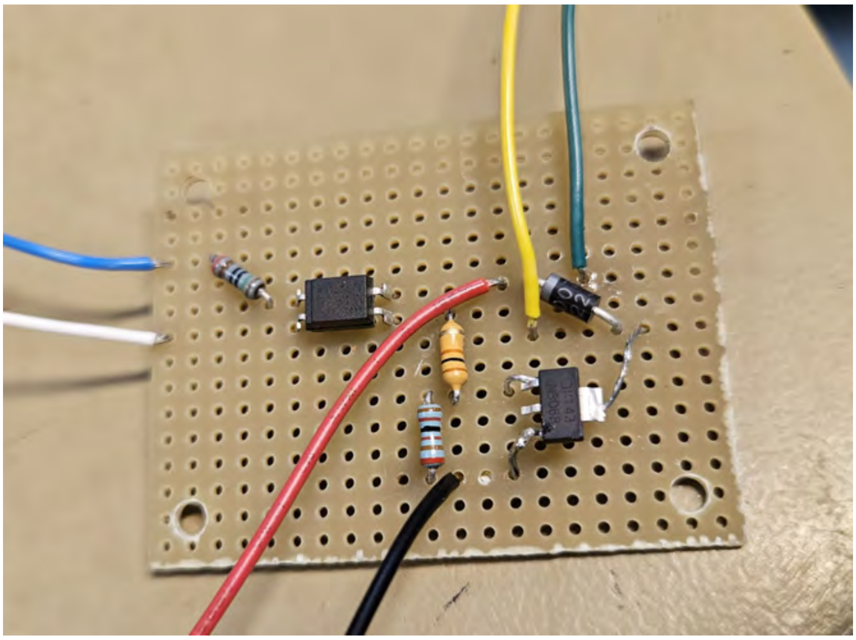

Figure 5.21: The relay drive circuit, consisting of an optocoupler with control signal wires (blue and white), 5 V input (red and black wires), relay connections (green and yellow) with freewheeling diode, and a MOSFET switch.

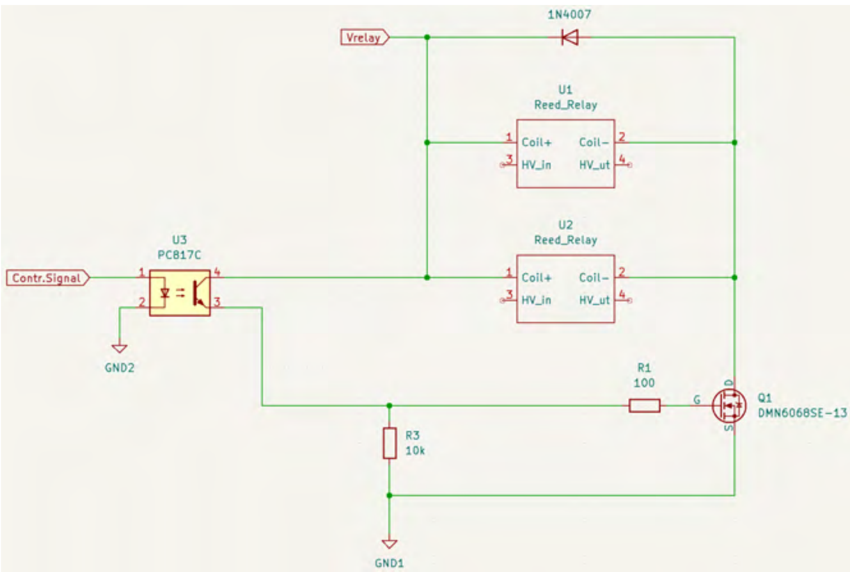

Figure 5.22: Schematic of the relay drive circuit, showing the connections of the optocoupler, relays and MOSFET.

The drive circuit was made on an experimental circuit board. To activate the relays a control signal is sent to the optocoupler, which initializes a 5 V signal to the gate of the MOSFET, turning it on. A current equal to 5 V divided by the internal coil resistance of the relays is sent through the coils, which activates them. Since the coils store energy a freewheeling diode is placed in parallel with the coils.

The contact operation of the relays are opposite each other, meaning that one will be open and the other will be closed when the coils are powered from the same source, and vice versa when the coils are not powered. This ensures that only one relay is activated all the time, and it also lowers the amount of components needed. However, it also means that zero current will be used in one case and twice as much will be used in the other case, compared to if two relays with the same contact operation principle were used instead, where the same current would be supplied all the time.

5.9 Isolated DC/DC converter

To provide isolated 5 V power, an isolated DC/DC converter is utilized. The assembled circuit is shown in Figures 5.23 and 5.24, and its schematic is presented in Figure 5.25.

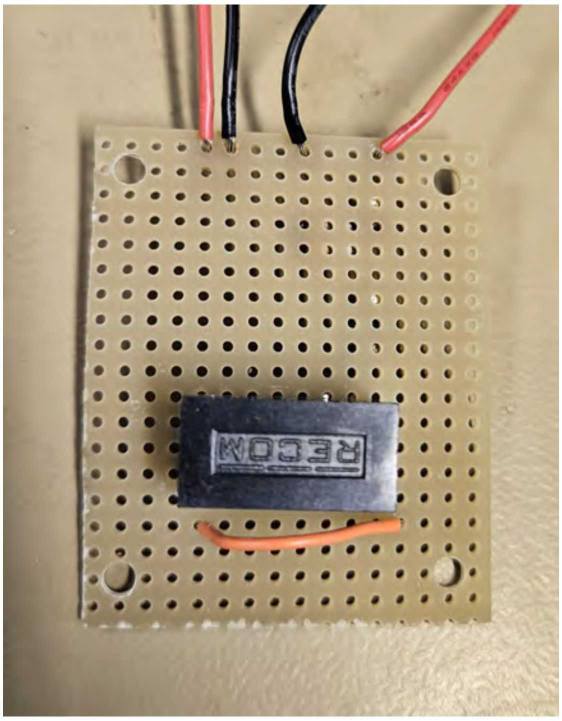

Figure 5.23: Top view of the isolated DC/DC converter circuit.

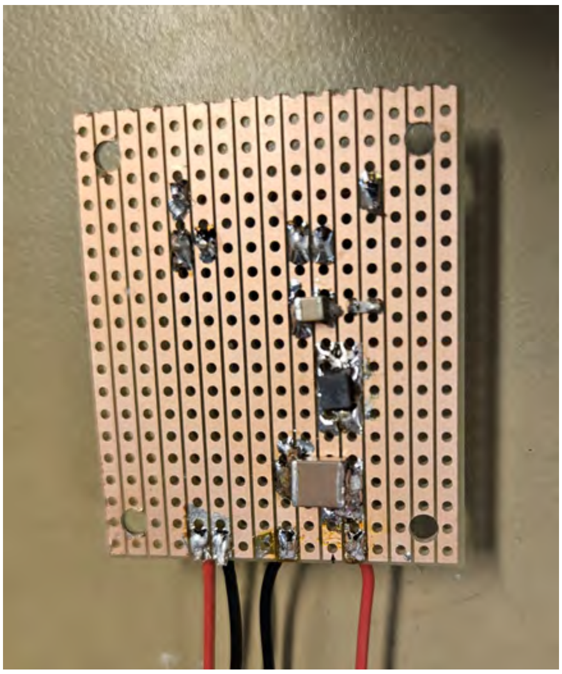

Figure 5.24: Bottom view of the isolated DC/DC converter circuit, showing the soldered filter components.

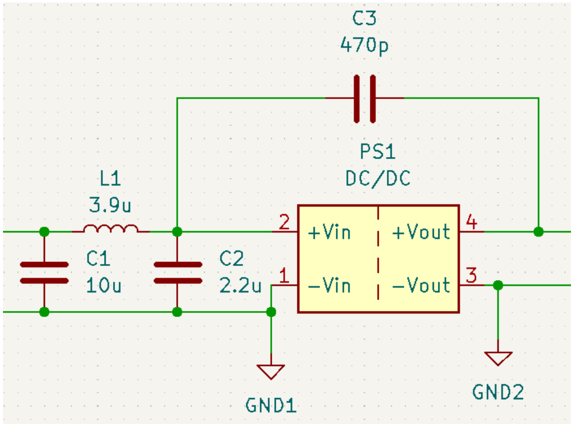

Figure 5.25: Schematic of the isolated DC/DC converter and filter.

The converter along with its filter is soldered onto an experimental circuit board. The filter design was described in the converter datasheet [23].

5.10 Controller

To ensure easy operation of the generator, a variety of buttons and a liquid crystal display (LCD) will be used to create a simple interface for the test operator. Therefore, a microcontroller is used to control these applications. The microcontroller utilized in this project is the STM32 Nucleo, which is shown together with the LCD display in Figure 5.26.

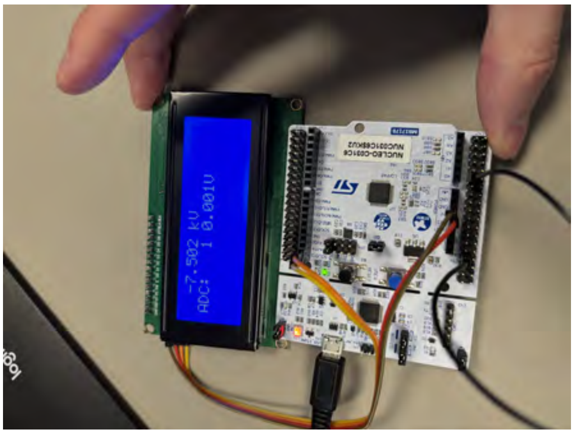

Figure 5.26: STM32 Nucleo microcontroller with an LCD display.

Figure 5.26 shows how the microcontroller displays the voltage level during operation. To measure the voltage in the charging capacitor a reinforced isolated amplifier with single-ended input of ± 12 V and differential output of ± 4 V is used together with a voltage divider that steps the voltage level down to 0-3.3 V. This enables direct measuring to the analog pins on the microcontroller. Instead of procuring a separate isolated DC/DC converter and integrating decoupling capacitors, an evaluation module (EVM) is utilized. This ensures that the voltage measurement is integrated into the system rapidly with minimal complications.

The microcontroller is also used to activate the triggered switch S_1 in the ring wave generator. An external button is utilized to activate the switch through an optocoupler and a MOSFET, which isolates the microcontroller from the high-voltage side.

Furthermore, the controller is used to switch between the output resistors. This signal is controlled with an external rotary switch and isolated with an optocoupler and a MOSFET. The signal connects to the two reed relays, which switches between the output resistors.

5.11 High-Voltage Measurement

To measure the voltage across the charging capacitor bank C_1, the high-voltage divider in Figure 5.27 is used. The divided voltage is sent to an EVM, shown in Figure 5.28.

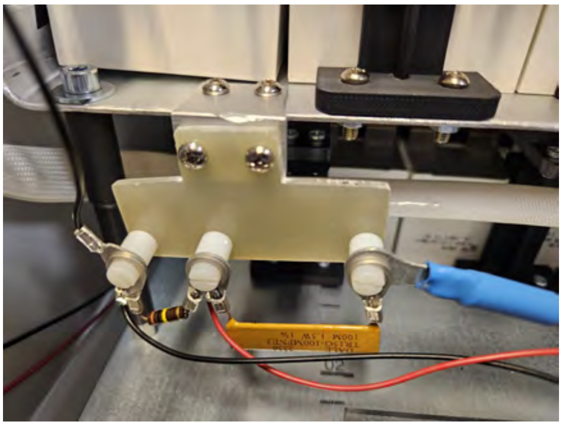

Figure 5.27: Mounted high-voltage divider circuit connected to the positive- (blue wire) and negative (black wire) nodes of C_1 with an output to the EVM (red and black wires).

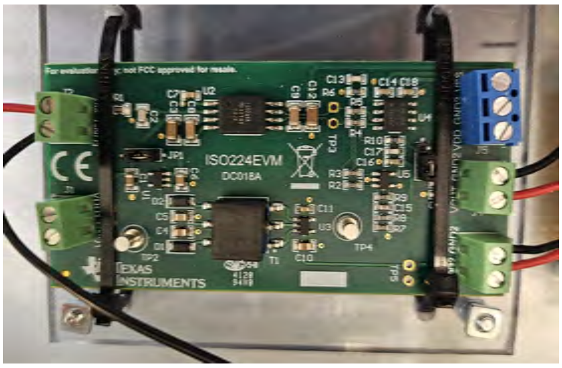

Figure 5.28: The Isolated EVM, used for measuring the voltage over C_1, zip tied to a plexiglass platform.

The high-voltage measurement has been designed to measure voltages between ±7.5 kV. It is composed of a 100 MΩ high-voltage resistor and a 100 kΩ resistor, providing a 1000:1 division. The voltage signal is transmitted to the EVM, which has an isolation up to 7 kV. The EVM converts the analog voltage signal from ±7.5 V into an isolated analog voltage signal between 0-5 V. It is then connected to another voltage divider with values of 3.3 kΩ and 6.8 kΩ this ensures that the voltage level from this voltage divider is between 0-3.3 V. This voltage divider is then connected to one of the analog pins on the microcontroller, which can measure the voltage between 0-3.3 V.

5.12 User interface

The front and back sides of the user interface (UI) on the generator are shown in Figure 5.29 and 5.30, respectively.

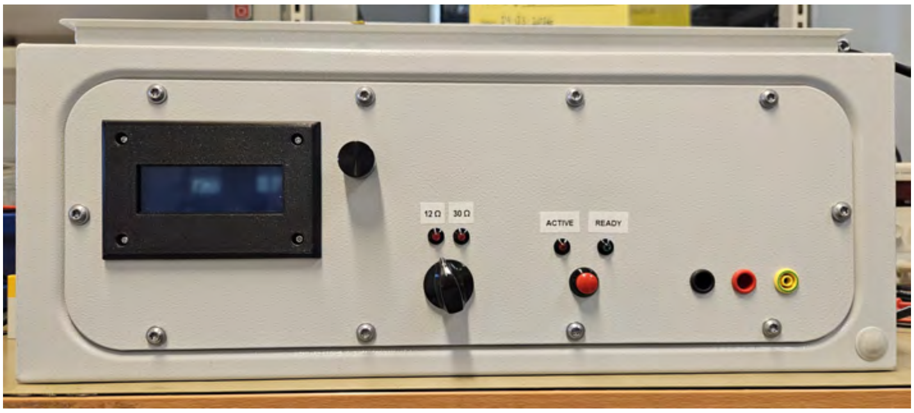

Figure 5.29: Front side UI of the ring wave generator, consisting of an LCD screen, a rotary encoder, rotary switch with LEDs, button with LEDs, and positive, negative and protective earth output ports.

Figure 5.30: Back side UI of the ring wave generator, consisting of a rocker switch with LED, 5 V barrel jack and the high-voltage source connecting wires.

The UI has an LCD display which is attached to a 3D-printed frame and the chassis. To the right of the LCD a rotary encoder is placed. For the moment being, the encoder is not connected to anything and cannot be used. However, it is meant to control different settings displayed on the LCD screen in the future. To select output resistor, a rotary switch is used. A diode is lit depending on which resistor is selected.

To start the ring wave discharge process a red button can be pressed. When pressed, a three second delay starts and a red diode lights up to show that the firing process is active. After the delay the controller triggers the GDT switch to discharge C_1 and create a ring wave. After the ring wave has been fired a green diode lights up, stating that the process is finished and ready to go again. Three outputs are available on the generator, positive, negative and protective earth.

On the rear of the generator, it is powered through a 5 V barrel jack. A rocker switch can be used to turn on and off the power. When the power is on, a light emitting diode (LED) will light up, showing that the generator is powered. On the right side a panel is placed where the cables that are used to charge the capacitor bank come through and are connected. These cables have 20 kV insulation.

5.13 Simulations

Simulations were conducted in LTspice to choose component values. The circuit in Figure 5.31 uses the final measured values. Figure 5.32 and 5.33 show the open-circuit voltage and short-circuit current, respectively.

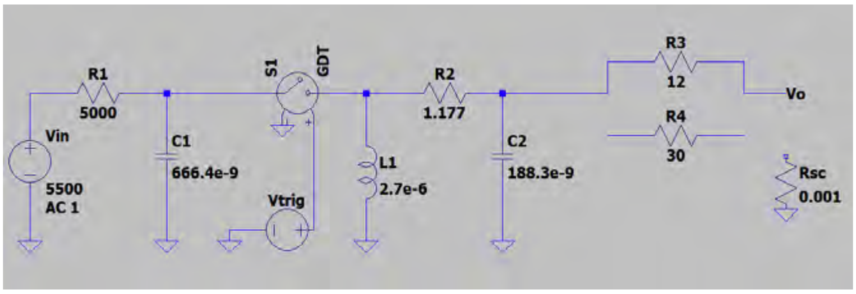

Figure 5.31: Simulation circuit of the ring wave generator.

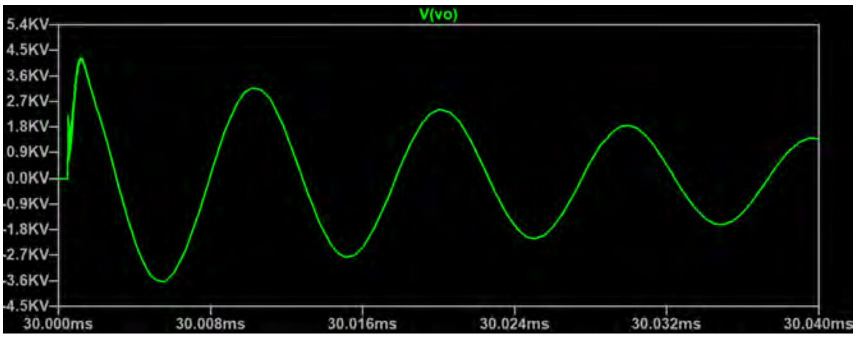

Figure 5.32: Simulation of the open-circuit output voltage from the ring wave circuit using the 12 Ω output resistor.

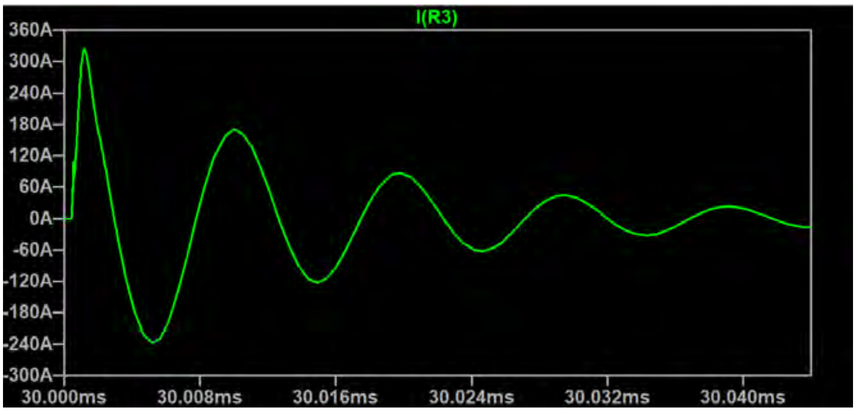

Figure 5.33: Simulation of the short-circuit current from the ring wave circuit using the 12 Ω output resistor.

The simulation shows the open-circuit ring wave which is marginally underdamped. The first peak reaches 4.2 kV. This was done on purpose, since the added wiring resistance and parasitic inductance was thought to damp the waveform further and to not overdamp the short-circuit case, as it is naturally more damped. The rise time is approximately 400 ns, and the frequency is 102.2 kHz. The peak ratios are as follows: Pk2/Pk1 = 0.86, Pk3/Pk2 = 0.88 and Pk4/Pk3 = 0.87.

The short-circuit case is well damped compared to the open-circuit case. The short-circuit current reaches 323 A, has a rise time of about 448 ns and an oscillation frequency of 103.3 kHz. The peak ratios are as follows: Pk2/Pk1 = 0.73, Pk3/Pk2 = 0.72 and Pk4/Pk3 = 0.72.

5.14 Ring wave test

Measurements were conducted on the ring wave generator to verify that the waveforms comply with the standard [4]. The setup can be viewed in Figure 5.34.

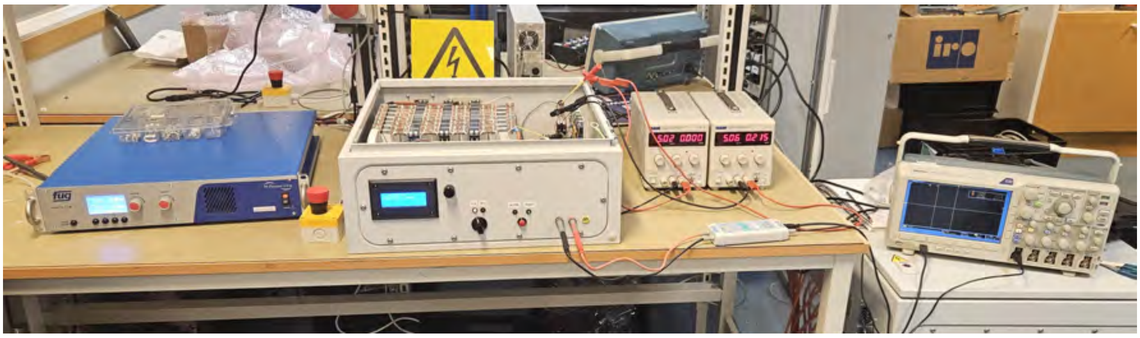

Figure 5.34: Test setup for the open-circuit ring wave measurements. The high-voltage source is connected to the generator charging resistors and the negative terminal of C_1. The 5 V voltage sources are connected to the low voltage input, and an oscilloscope with the high-voltage probe is connected to the output ports of the generator.

The 10 kV source is connected to the rear cables to enable charging of the capacitor bank. In this case, the 5 V to the low voltage part of the generator was provided by two smaller power sources connected in parallel. Two sources are utilized because a single unit can only supply 3 A, whereas a higher current is required. The high-voltage probe is connected to the positive and negative output ports of the generator, and to an oscilloscope. An emergency stop button is placed to the left of the generator for safety. A 2 kV open-circuit measurement can be seen in Figure 5.35.

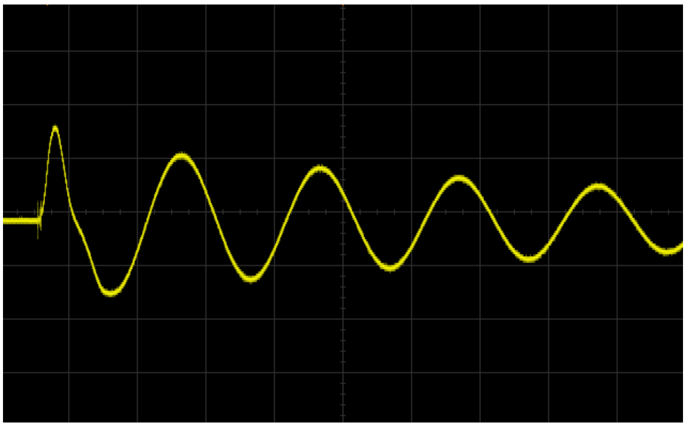

Figure 5.35: Measurement of a 2 kV ring wave.

The waveform looks similar to the simulations. The first period has some irregularities, but overall the wave has nice and clear oscillations. It is more damped than the simulations as expected. However, it is still slightly underdamped. Table 5.1 shows the open-circuit measurement results from the ring wave generator after assembly. According to Table 5.1, the peaks are within the specified tolerance of ±10%, which is defined by the ring wave standard [4]. The rise time is slightly too long. According to the standard [4] it should be 0.5 µs ±30%. The decaying peak ratios should be between 0.4-1.1 for Pk2/Pk1, and 0.4-0.8 for Pk3/Pk2 and Pk4/Pk3. The frequency should be 100 kHz ±10%.

Table 5.2 shows the short-circuit measurement results, with the 12 Ω output resistor connected. According to Table 5.2 the peaks rise time is below 1 µs which is the short-circuit condition according to the standard [4]. The peak ratios complies with the requirements of 0.4-1.1 for Pk2/Pk1, and 0.4-0.8 for Pk3/Pk2 and Pk4/Pk3. The frequency is within 100 kHz ±10 %.

The peak-to-peak ratios from the measurements in Table 5.1 and 5.2 show that the ring wave generator produces ring waves that are marginally underdamped in the open-circuit case, and well damped in the short-circuit measurements. This means that some damping could be added to the circuit to increase the decaying. However, the configuration for this generator omitted additional damping, as distinct waveforms were preferred, and because tests at lower voltage levels were more damped. When the final measurements were conducted it was clearly observed that damping decreased when the voltage level increased. However, the controller was damaged during the higher voltage tests and no further measurements could be taken for the

Table 5.1: Open-circuit ring wave measurements using the 12 Ω output resistor.

Level	Peak	Risetime	Pk2/Pk1	Pk3/Pk2	Pk4/Pk3	Freq.
250 V	276 V	720 ns	0.80	0.73	0.73	93.6 kHz
500 V	488 V	720 ns	0.80	0.80	0.82	93.3 kHz
1 kV	1024 V	720 ns	0.86	0.80	0.80	95.4 kHz
2 kV						
4 kV						

Table 5.2: short-circuit ring wave measurements using the 12 Ω output resistor.

Level	Peak	Risetime	Pk2/Pk1	Pk3/Pk2	Pk4/Pk3	Freq.
250 V	19,2 A	760 ns	0,75	0,56	0,55	94,3 kHz
500 V	33,6 A	720 ns	0,75	0,65	0,71	95,0 kHz
1 kV	72 A	800 ns	0,72	0,73	0,71	95,4 kHz
2 kV	138 A	840 ns	0,74	0,71	0,64	96,5 kHz
4 kV						

time being.

5.15 Reliability of the GDT switch

One of the main problems is the reliability of the GDT switch. Sometimes the switch would not work, but a sound could still be heard. If this was due to the GDTs or something else is unclear. The flyback trigger can deliver sufficient voltage to fire all utilized GDTs; however, since triggering failed, it remains unclear whether the GDT had reached its end-of-life or if breakdown occurs elsewhere. The GDTs were measured when they were connected to the flyback individually, and most did get consistent breakdown, showing that they have not reached their end-of-life. When connecting everything back together the trigger was unsuccessful yet again. At another time one GDT did get very uneven breakdowns when individually connected to the flyback, showing that it did not work properly. Accordingly, the unsuccessful triggering could be due to bad GDTs, but at other times due to something else.

In the early testing of the flyback it was viewed that an open circuit connection on the output, would result in a breakdown in the transformer windings of the flyback. However, it was not the case for voltages lower than 6 kV. This was also not seen during the latest ring wave tests. It should not be possible to get breakdown through the lower rated GDT either, since the flyback voltage needs to be higher than the rated voltage of lower rated GTD plus the voltage of the charged capacitor bank, meaning that the flyback should only trigger the higher rated GDT. The possibility of a breakdown within the flyback circuit exists and must be investigated, particularly since the controller was destroyed at the highest voltage levels. If the problem is found, more consistent triggering could be possible.

5.16 Ethical and environmental aspects

When designing and building a product it is important to take ethical and environmental aspects into consideration. As this project seeks to build a high-voltage product it is especially important to ensure ethical and safe design, and to seek to minimize the environmental impact of the finished product.

In accordance with IEEE code of ethics policy number 1 [21]. This project has sought to minimize the environmental impact of the generator by taking end of life disposal into account. To minimize material use and to choose components with lower environmental impact where possible.

Operational safety is something to take into account, as the ring wave generator can produce ring waves up to 4 kV, while the capacitor bank C_1 is charged up to 5,5 kV. This poses a serious safety risk to the test operator; therefore, the designers have an ethical duty to implement safeguards, such as enclosures and discharge circuits. Documentation and training obligations extend beyond the designers to anyone who will maintain and use the equipment. There can also be a dual use risk of a ring wave generator. It is supposed to be used to test equipment against ring waves, but theoretically it could also be used to stress grid connected equipment and potentially cause harm to the grid. This is a minor risk, but it should be taken into consideration when produced and stored. These factors are consistent with IEEE principles of avoiding injuring others, and their property. Which is described under policy 9 [21].

As more critical systems are connected to the grid, the importance of transient immunity increases to protect these systems from damage and failure. So creating testing equipment for transient immunity is a contribution to create higher societal resilience against grid disturbances and a more reliable energy system. There is also a societal dimension of who can afford compliance testing. As this generator is built for a small company, which has limited resources. This generator will help to increase the availability of EMC test compliance equipment. Smaller companies may not have the resources to visit external test labs for validation tests multiple times. Thus by increasing accessibility to transient testing equipment this project aligns with IEEEs code of ethics policy 2 which strives to improve the understanding by individuals and society of the capabilities and societal implications of conventional and emerging technologies [21].

6
Conclusion

To conclude, the results from the ring wave testing reveal that the rise time under open-circuit conditions, measured at 720 ns, is above the requirement of 650 ns. However, the remaining requirements were met. Comparing the experimental results with simulations, both the rise time and overall waveform damping were found to be higher in practice than predicted. This is consistent with expected real world behavior. In the simulation phase of this thesis it was discovered that even small amounts of resistance introduce significant damping, while parasitic inductance in the vicinity of the RC filter contributes to increased rise times. The challenge throughout the design phase, however, was to accurately predict the parasitic elements that would manifest in the fully assembled generator.

The Bode measurements show that the SRF of all components is above 100 kHz. However, the rise time has a frequency much larger than 100 kHz, up to around 500 kHz, meaning that the components will operate much closer to their respective SRF during the rise. The capacitor bank C_1 operates especially close to its SRF here, which may influence the waveform. The ripple in the rise time, shown in both the simulation and the measurement waveforms, likely stem from this.

The assembled components were measured and verified to work according to expectations. All of them withstood the ring wave testing, and together they produce highly satisfactory ring waves. The measured parasitics in the components were low and incorporated into the simulations, which produced a wave that still looked satisfactory. This proves that the decisions made in the design process of the components were effective and justified.

In the short-circuit measurement it is observed that the peak ratios become much smaller in the 250 V test. A small difference can also be seen in the open-circuit case. This is a behavior that is not seen in the simulations. The causes for the difference in peak ratios were not further investigated, but it was noted that by increasing the voltage level the peak ratios also increased.

One of the primary challenges encountered in this thesis was the selection of an appropriate switch S_1, capable of withstanding voltages up to 6 kV, currents up to 5 kA, and operating frequencies exceeding 100 kHz, while simultaneously exhibiting a very low on-state impedance and fast, jitter-free turn-on behavior. A survey of commercially available solutions revealed that devices meeting these specifications exist only in highly specialized market segments, and consequently carry a significant cost premium. Given these constraints, designing and constructing a triggered spark gap was identified as a viable and cost-effective alternative worth pursuing.

The triggered spark gap that was subsequently constructed demonstrated promising results, producing a well-defined output waveforms. However, the consistency of the triggering remained relatively low, representing the primary limitation of the implemented design and an area warranting further development.

6.1 Future work

Several aspects of the ring wave generator could be further developed. The primary improvement should involve integrating control of the high-voltage power supply into the ring wave generator. This could be done by using the serial interface for remote control on the high-voltage power supply, and connecting it to the controller in the ring wave generator. The voltage level could then be controlled by the rotary encoder, placed next to the LCD screen. However, implementing the control logic for the rotary encoder and programming what is shown on the screen are other aspects that must be addressed.

An additional function that could be implemented is the possibility to choose how many pulses to fire in a test. According to the standard [4] the density of pulses could vary between 1 and 60 pulses per minute. The ring wave generator built in this project is designed with the potential to produce from 1 to 60 pulses per minute. However, the software must be finalized, and the ability to control the high-voltage supply directly from the microcontroller would greatly enhance the possibility for this feature. Otherwise, an operator must manually maintain the charge on C_1 for one minute while the pulses are triggered.

Furthermore, eliminating the reliance on an external high-voltage power source would be highly advantageous, as these units are often in demand and in limited supply at Aros. Therefore, it would be great if a high-voltage power source could be directly built and integrated into the ring wave generator.

From the results in Table 5.1 it can be seen that the rise time is too slow according to the standard [4]. Therefore an improvement should be to reduce the rise time to meet the requirement of the standard. The peak ratios in the open-circuit case indicate an underdamped response; thus, adding minor damping could be beneficial.

The protection of the microcontroller should also be sought to be improved, since it is located close to the ring wave circuit it may be severely affected by electromagnetic interference. An improvement would be to shield the microcontroller, and to use fiber optic cables instead of ordinary copper wires from the microcontroller to ensure maximum isolation. Additionally, protection circuits could be implemented within the low-voltage switching circuits.

A safety feature that could be added is an emergency button that stops the high-voltage power source from charging the capacitor bank, immediately discharges the bank and stops the triggering. This feature is extra important if the possibility to fire multiple consecutive pulses is implemented.

Further investigation into improving the triggering reliability of the triggered spark gap would be a natural continuation of this work. While the spark gap successfully produced well defined damped sinusoidal waveforms, the triggering consistency was found to be insufficient for dependable operation. The gap exhibited variable behavior; occasionally, it would fire on the first attempt, whereas at other times, multiple attempts were required before successful triggering. Identifying and addressing the root causes of this variability, would be an important step toward making the spark gap a robust and repeatable switching solution.

Bibliography

[1] F.Martzloff and G.Pellegrini, "Real, Realistic Ring Waves for Surge Testing," in *Proc. 1991 Electromagnetic Compatibility (EMC) Symposium*, Zurich, Switzerland, 1991, pp. 499-504. [Online]. Available: https://www.nist.gov/system/files/documents/pml/div684/Real_Waves.pdf

[2] P.Poungsri and A.Singhasathein, "The design of simulation and the creation of a combination wave and ring wave generator in accordance with the international standard IEC 61000-4-5 and IEC 61000-4-12," in *2019 7th International Electrical Engineering Congress (iEECON)*, Hua Hin, Thailand, 2019, pp. 1-4. [Online]. Available: https://ieeexplore.ieee.org/document/8938935

[3] *IEEE Standard for Surge Withstand Capability (SWC) Tests for Relays and Relay Systems Associated with Electric Power Apparatus*, IEEE Std C37.90.1, 2012.

[4] *International Electrotechnical Commission, Electromagnetic compatibility (EMC) – Part 4-12: Testing and measurement techniques – Ring wave immunity test*, IEC 61000-4-12, 2017.

[5] J. Luo, L. Tang, and C. Xu, "An alternative high-voltage switch consisting of gas discharge tubes (GDTs) for high-power pulse applications," *Rev. Sci. Instrum.*, vol. 96, no. 5, p. 054708, May 2025. doi: https://doi.org/10.1063/5.0246529,

[6] PROSEMI, "Gas Discharge Tube (gdt) Explained: Principles, Applications, And Selection Guide", 2025. [Online]. Available: https://www.prosemicsr.com/industrial-application/gas-discharge-tube-gdt-explained-principles-applications-and-selection-guide

[7] HOFSTAgroup, "Triggered spark gap design." [Online]. Available: https://hofstragroup.com/triggered-spark-gap-design.html. [Accessed: May 11, 2026].

[8] FuG Elektronik GmbH, *M-Power-Line - Compact High-Voltage Power Supply Unit: Datasheet for part MPL 1000-10000.* [Online]. Available: https://smt.at/wp-content/uploads/smt-datenblatt-fug-mpl-datenblatt-englisch.pdf

[9] Power Elektronik Measurements Ltd, *CWT Ultra-mini: Datasheet for part CWTUM/3.* [Online]. Available: https://www.pemuk.com/uploads/files/datasheets/CWT-Ultra-mini-datasheet.pdf?v=1760953930

[10] Micsig Technology, *High Voltage Differential Probe: Datasheet for part DP20003.* [Online]. Available: https://www.micsig.com/uploads/HighVoltageDifferentialProbeUserManual_1656560834.pdf

[11] Analog Devices, "LTspice", 2025. [Online]. Available: https://www.analog.com/en/resources/design-tools-and-calculators/ltspice-simulator.html

[12] STMicroelectronics, "STM32CubeIDE", 2026. [Online]. Available: https://www.st.com/en/development-tools/stm32cubeide.html

[13] KiCad, "KiCad", 2026. [Online]. Available: https://www.kicad.org/

[14] MATLAB, "MATLAB", 2026. [Online]. Available: https://se.mathworks.com/products/matlab.html

[15] KEMET Electronics Corporation, *IGBT Direct Mount Power Film Capacitors C4BS, 850–3000 VDC/550–750 VAC: Datasheet for part C4BSYBX3470Z(3)M*. [Online]. Available: https://yageogroup.com/content/datasheet/asset/file/KEM_F3048_C4BS

[16] KEMET Electronics Corporation, *IGBT Direct Mount Power Film Capacitors C4BS, 850–3000 VDC/550–750 VAC: Datasheet for part C4BSYBX3330Z(3)LJ*. [Online]. Available: https://yageogroup.com/content/datasheet/asset/file/KEM_F3048_C4BS

[17] Sensata Technologies, *D SERIES | HIGH VOLTAGE RELAYS 10KV* & *15KV: Datasheet for part DBR70510* & *DAR70510*. [Online]. Available: https://www.cynergy3.com/sites/default/files/sensata-reed-relay-d-series-pcb-datasheet.pdf

[18] V. Sung and W. G. Odendaal, "Litz Wire Pulsed Power Air Core Coupled Inductor," in IEEE Transactions on Industry Applications, vol. 51, no. 4, pp. 3385-3393, Mar. 16, 2015. [Online]. Available: https://ieeexplore.ieee.org/document/7061416

[19] W. C. Young and R. G. Budynas, "Shells of Revolution; Pressure Vessels; Pipes," in *Roark's formulas for stress and strain*, 7th Ed., New York, NY, USA: McGraw-Hill, 2001, ch. 13, sect. 13.8, pp. 592. [Online]. Available: https://www.vlebooks.com/Product/Index/1943717?page=0&startBookmarkId=-1

[20] L. Zhang, Z. Zhao, R. Jin, X. Yang, X. Li and X. Cui, "SiC MOSFET Turn-Off Measurement With Air-Core Inductor Design and RC Snubber Correction," in IEEE Transactions on Instrumentation and Measurement, vol. 74, pp. 1-13, Feb. 25, 2025. [Online]. Available: https://ieeexplore.ieee.org/document/10902149

[21] IEEE, "IEEE Code of Ethics," *IEEE*, 2020. [Online]. Available: https://www.ieee.org/about/corporate/governance/p7-8. [Accessed: May 9, 2026].

[22] S. Zurek, "Ayrton-Perry winding", in *Encyclopedia Magnetica*, 2021, [Online]. Available: https://www.e-magnetica.pl/doku.php/ayrton-perry_winding, Accessed on: 2026-03-23.

[23] Recom Power, *DC/DC Converter RxxP2xx/R, 2 Watt SIP 7 Single and Dual Output: Datasheet for part R05P205S/P/X2/R8*. [Online]. Available: https://recom-power.com/pdf/Econoline/RxxP2xx_R.pdf

DEPARTMENT OF ELECTRICAL ENGINEERING
CHALMERS UNIVERSITY OF TECHNOLOGY
Gothenburg, Sweden
www.chalmers.se